NEURODEGENERATIVE DISEASE



# A farnesyltransferase inhibitor activates lysosomes and reduces tau pathology in mice with tauopathy

**Israel Hernandez[1]*, Gabriel Luna[1]*, Jennifer N. Rauch[1], Surya A. Reis[2], Michel Giroux[1], Celeste M. Karch[3], Daniel Boctor[1], Youssef E. Sibih[1], Nadia J. Storm[4], Antonio Diaz[4], Susmita Kaushik[4], Cezary Zekanowski[5], Alexander A. Kang[1], Cassidy R. Hinman[1], Vesna Cerovac[1], Elmer Guzman[1], Honjun Zhou[1], Stephen J. Haggarty[2], Alison M. Goate[6], Steven K. Fisher[1,7], Ana M. Cuervo[4], Kenneth S. Kosik[1,7]†**

**Tau inclusions are a shared feature of many neurodegenerative diseases, among them frontotemporal dementia caused by tau mutations. Treatment approaches for these conditions include targeting posttranslational modifications of tau proteins, maintaining a steady-state amount of tau, and preventing its tendency to aggregate. We discovered a new regulatory pathway for tau degradation that operates through the farnesylated protein, Rhes, a GTPase in the Ras family. Here, we show that treatment with the farnesyltransferase inhibitor lonafarnib reduced Rhes and decreased brain atrophy, tau inclusions, tau sumoylation, and tau ubiquitination in the rTg4510 mouse model of tauopathy. In addition, lonafarnib treatment attenuated behavioral abnormalities in rTg4510 mice and reduced microgliosis in mouse brain. Direct reduction of Rhes in the rTg4510 mouse by siRNA reproduced the results observed with lonafarnib treatment. The mechanism of lonafarnib action mediated by Rhes to reduce tau pathology was shown to operate through activation of lysosomes. We finally showed in mouse brain and in human induced pluripotent stem cell–derived neurons a normal developmental increase in Rhes that was initially suppressed by tau mutations. The known safety of lonafarnib revealed in human clinical trials for cancer suggests that this drug could be repurposed for treating tauopathies.**

## INTRODUCTION

The tauopathies constitute a broad range of neurodegenerative diseases, all of which share the hallmark feature of tau inclusions. Although tau-related diseases including Alzheimer's disease and chronic traumatic encephalopathy are serious public health problems *(1)*, no disease-modifying treatment currently exists for these conditions. Generally, approaches to treatment have directly targeted the tau protein and include tau antibodies *(2)*, antisense oligonucleotides *(3)*, caspase cleavage products *(4)*, and anti-aggregation agents *(5)*. However, few pharmacologic interventions directed toward tau pathways have reached clinical trials. Interventions in upstream pathways such as inhibitors of tau phosphorylation *(6)* or acetylation *(7)* have shown some efficacy in animal models, but none of these approaches has had success in human clinical trials to date. Rapidly growing interest in autophagy as a downstream pathway that mediates tau clearance *(8–10)* as well as the implication of autophagy and lysosomes in other neurodegenerative conditions *(11–13)* suggest therapeutic opportunities. In Huntington's disease (HD), a pathway linked to autophagy is mediated by the *RASD2* gene, which encodes the Rhes protein, a small guanosine triphosphatase (GTPase) member of the Ras superfamily *(14)*. *RASD2* became of interest in HD because it was thought to be expressed mainly in the striatum *(15)*. However, in humans, Rhes expression is clearly evident in the cerebral cortex *(16)*. Rhes activates autophagy independently of mammalian target of rapamycin (mTOR) via interaction with beclin 1 *(17)*. Furthermore, Rhes has been shown to modulate the aggregation state of mutant Huntingtin (mHtt), the protein mutated in HD, by promoting its sumoylation and reducing cell survival *(18)*. This toxicity involves binding of Rhes to mHtt and requires the Rhes CXXX farnesylated membrane attachment site *(18)*. We inferred that the induction of autophagy is a pharmacological class effect of farnesyltransferase inhibition *(19)* and could be relevant for tauopathies. Therefore, we studied farnesyltransferase as a therapeutic target for the treatment of tauopathies. We used the farnesyltransferase inhibitor lonafarnib, a drug for which there is extensive clinical experience *(20–22)*, and tested it in the rTg4510 mouse model of tauopathy.

## RESULTS

### Farnesylation inhibition attenuates tau pathology in the rTg4510 mouse model of tauopathy

Lonafarnib is a potent farnesyltransferase inhibitor with a $K_i$ (inhibition constant) in the nanomolar range *(23)*, which crosses the blood-brain barrier and has only a few minor side effects in humans (*21*). We sought to determine the effects of lonafarnib administration in the rTg4510 mouse, a widely used model of frontotemporal dementia *(24)*. These mice develop tau tangles in the cerebral cortex by 4 months of age and in the hippocampus by 5.5 months of age along with the loss of about 60% of their hippocampal CA1 neurons *(24)*. Spatial memory deficits become apparent by 2.5 to 4 months of age, and electrophysiological properties of cortical neurons are affected before the accumulation of tau pathology *(25, 26)*. To precisely determine

[1]Neuroscience Research Institute, University of California, Santa Barbara, Santa Barbara, CA 93106, USA. [2]Department of Neurology, Massachusetts General Hospital, Chemical Neurobiology Lab, and Center for Genomic Medicine, Harvard Medical School, Boston, MA 02114, USA. [3]Department of Psychiatry, Washington University School of Medicine in St. Louis, St. Louis, MO 63110, USA. [4]Department of Developmental and Molecular Biology and Institute for Aging Studies, Albert Einstein College of Medicine, New York, NY 10461, USA. [5]Laboratory of Neurogenetics, Mossakowski Medical Research Centre, Polish Academy of Sciences, 5 Pawinskiego St., 02-106 Warsaw, Poland. [6]Department of Neuroscience, Icahn School of Medicine at Mount Sinai, New York, NY 10029, USA. [7]Department of Molecular, Cellular, and Developmental Biology, University of California, Santa Barbara, Santa Barbara, CA 93106, USA.
*These authors contributed equally to this work.
†Corresponding author. Email: kenneth.kosik@lifesci.ucsb.edu

the effects of lonafarnib, we first replicated the time course for the onset of tau pathology in rTg4510 mice (Fig. 1, A to K, and fig. S1). Similar to the reported data, immunoreactivity for the conformational tau antibody MC1, corresponding to neurofibrillary tangles throughout the hippocampus, amygdala, entorhinal cortex, and cerebral cortex (Fig. 1A, green), was first detected at ~16 weeks of age (fig. S1D). Immunoreactivity progressed by 20 weeks of age to a mean of 93.0 ± 13.6 MC1-positive cells/mm$^2$ in the cerebral cortex and 67.6 ± 13.1 MC1-positive cells/mm$^2$ in the hippocampus (Fig. 1, D and E). Wild-type (WT) mice showed no detectable MC1-positive neurons (Fig. 1C).

Lonafarnib treatment was initiated at 10 weeks of age. Lonafarnib was resuspended in 20% 2-hydroxypropyl-β-cyclodextrin as vehicle, and rTg4510 mice were gavaged on an intermittent schedule, with 5 days on and 5 days off at 80 mg/kg per day *(27)*. Mice were evaluated at 20 weeks of age (Fig. 2, A to H) and showed that drug treatment reduced MC1 immunoreactivity. The MC1 immunoreactivity in the lonafarnib-treated mouse cortex (88.8 ± 8.1 MC1-positive cells/mm$^2$) and hippocampus (27.4 ± 5.2 MC1-positive cells/mm$^2$) was significantly reduced compared to either vehicle-treated mice (183.3 ± 10.4 MC1-positive cells/mm$^2$ in the cortex and 82.2 ± 6.8 MC1-positive cells/mm$^2$ in the hippocampus; cortex: $P = 0.006$, hippocampus: $P = 0.001$; Fig. 2H) or untreated age-matched transgenic mice (cortex: $P = 0.049$, hippocampus: $P = 9.6 \times 10^{-6}$). Comparable results were obtained by immunostaining mouse brain sections with the phospho-tau antibody PHF-1 (cortex: $P = 3.2 \times 10^{-4}$, hippocampus: $P = 3.59 \times 10^{-5}$; fig. S2, A to F). Farnesyltransferase activity was inhibited in the brains of lonafarnib-treated mice, as determined by the appearance of an unfarnesylated heat shock protein HDJ-2 band in cortical lysates, but was not observed in untreated rTg4510 mice (fig. S2G). The presence of the unfarnesylated band in mice treated with vehicle alone remains unexplained. In contrast to chronic administration, lonafarnib was ineffective as an acute intervention. rTg4510 mice gavaged daily with lonafarnib for 2 weeks (80 mg/kg per day), beginning at 20 weeks of age when tau pathology was widespread, failed to alter the location and extent of the MC1-immunostained pathology when compared to age-matched vehicle-treated transgenic mice (fig. S3).

Chronic lonafarnib treatment also prevented the reduction in brain size among aged transgenic mice. The brain coronal section area of littermate controls and transgenic mice did not differ at 5 weeks of age but diminished by 20 weeks as the mice aged (Fig. 1B). Lonafarnib-treated rTg4510 mice at 20 weeks of age had larger coronal brain areas than either vehicle-treated or untreated age-matched transgenic mice [$P = 1.3 \times 10^{-3}$, analysis of variance (ANOVA); Fig. 2A].

Microglia counts, assessed by Iba1 immunostaining at 5 and 20 weeks of age (Fig. 1, F and G, and fig. S1), decreased with age (Fig. 1H) in the control mouse cortex ($P = 0.049$) and hippocampus ($P = 0.014$) but remained elevated in 20-week-old rTg4510 mice. At 5 weeks of age, no statistical difference was observed in microglial counts between control and transgenic mice. However, by 20 weeks, this difference was significant in both the cortex and hippocampus (cortex: $P = 0.019$, hippocampus: $P = 0.005$; Fig. 1H). Lonafarnib-treated 20-week-old rTg4510 mice (Fig. 2, I to L) had a significant reduction in hippocampal microgliosis compared to age-matched vehicle-treated transgenic mice ($P = 0.022$; Fig. 2M) but had no effect on cortical microgliosis ($P = 0.67$, ANOVA).

Cortical astrogliosis was observed in transgenic mice as increased glial fibrillary acidic protein (GFAP) immunoreactivity (Fig. 1A, red), which became apparent from ~12 weeks of age and preceded the appearance of MC1-positive neurons (fig. S1). As transgenic mice aged, anti-GFAP immunoreactivity increased in the cortex but not in the hippocampus (Fig. 1, I to K). Lonafarnib treatment decreased cortical astrocyte immunostaining when compared to vehicle-treated mice ($P = 0.041$; Fig. 2, N to R) but displayed no effect on the hippocampus ($P = 0.236$, ANOVA).

## Attenuation of behavioral abnormalities in rTg4510 mice by farnesyltransferase inhibition

As rTg4510 transgenic mice age, they display progressive behavioral impairments. Marble burial and nest shredding behaviors *(28, 29)* are affected early, and by 30 weeks of age, transgenic animals have progressed to hyperexcitability and obsessive circling. Using the same lonafarnib treatment protocol (*27*, *30*), beginning at 10 weeks of age, we sought to reduce or prevent the behavioral deficits induced by tau pathology. Nest building was assessed at 20 weeks. WT littermates produced well-rounded nests (Fig. 3A); however, untreated rTg4510 mice displayed poor nest shredding and, in some instances, left bedding material completely undisturbed (Fig. 3B). Lonafarnib treatment rescued nest building (Fig. 3C). At 5 weeks of age, littermate controls and transgenic mice produced nests with similar scores (control mice, 3.58 ± 0.13; transgenic mice, 3.23 ± 0.12; $P = 1.00$). Whereas control mice nesting scores did not significantly change with time ($P = 1.00$), transgenic mice nesting scores declined ($P = 1.9 \times 10^{-11}$; Fig. 3D). Twenty-week-old transgenic mice treated with lonafarnib had significantly higher nesting scores than vehicle-treated age-matched transgenic mice ($P < 3.3 \times 10^{-12}$) and did not differ from those of age-matched control mice ($P = 1.00$; Fig. 3D). On the other hand, the marble burial deficit was observable at 5 weeks in transgenic mice, and it remained unaltered by age (Fig. 3, E to G). In contrast to nest building, the marble burial deficit (Fig. 3, E and F) was not improved by the drug in the transgenic mice (Fig. 3H) when compared to vehicle-treated mice ($P = 1.00$) or untreated mice ($P = 0.231$). The very early emergence of the marble burial deficit before lonafarnib administration, in contrast to shredding behavior, which emerged later, may account for this difference. Lonafarnib does not appear to reverse existing pathology or behavioral deficits. rTg4510 mice exhibited circling behavior at 20 weeks of age. Lonafarnib appeared to prevent circling that lasted longer than 5 min at a time (movie S1). Circling was absent in control mice (observed in zero of six mice) and was frequently observed at 20 weeks of age in transgenic mice (five of six; $P = 3.42 \times 10^{-3}$). rTg4510 mice treated with vehicle continued to exhibit circling behavior (four of six; $P = 0.014$), whereas those treated according to the chronic intermittent lonafarnib regimen rarely developed this behavior (one of six; $P = 0.296$) and engaged in more normal exploratory behaviors in the testing cage (movie S1).

## Farnesyltransferase inhibition with lonafarnib enhances lysosomal protein degradation

To determine the mechanism of action of lonafarnib, we focused on its previously suggested role in autophagy *(31)*. Using NIH3T3 mouse fibroblasts expressing the tandem reporter mCherry–green fluorescent protein (GFP)–LC3B *(32)* to monitor macroautophagy (Fig. 4 and fig. S4), lonafarnib treatment resulted in a dose-dependent increase in macroautophagy flux, as revealed by an overall increase in autophagic vacuoles mostly due to an increase in autolysosome abundance. At lower concentrations, the number of autophagosomes

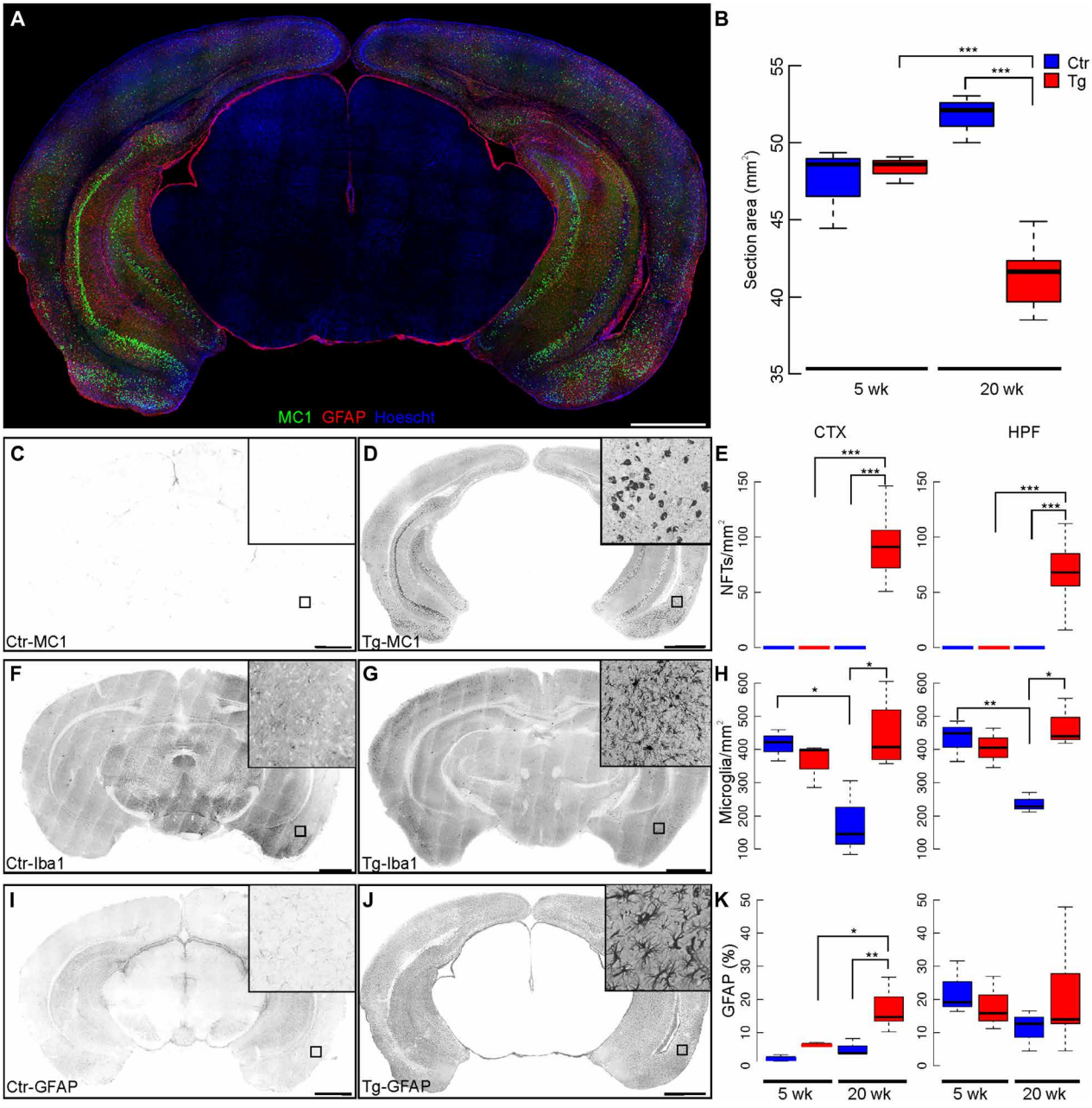


**Fig. 1. Baseline time course of tau pathology in the rTg4510 mouse model of tauopathy.** (**A**) Representative mosaic of a coronal section from rTg4510 mouse brain immunostained with MC1 antibody (green) or GFAP (red) and counterstained with Hoechst (cell nuclei, blue). (**B**) The coronal section area of the micrographs was computed. At 5 weeks of age, rTg4510 transgenic (Tg) mice did not differ in brain size from their nontransgenic littermates ($P = 0.942$). However at 20 weeks, the coronal section area was significantly reduced in transgenic mice compared to both age-matched controls and younger transgenic animals ($P = 6.94 \times 10^{-4}$). (**C**) Twenty-week-old control littermates (Ctr) show no immunostaining of brain tissue with MC1, (**D**) whereas 20-week-old transgenic mice show a high density of neurons strongly labeled with MC1 in both cerebral cortex (CTX) and hippocampal formation (HPF). (**E**) Quantification of neurofibrillary tangles (NFTs/mm$^2$) in the cortex and hippocampus. Representative micrographs showing microglia (Iba1-positive cells) in 20-week-old control (**F**) and transgenic (**G**) mice. (**H**) Quantification of microglia per square millimeter density reveals that there is no microglia age-related decline in rTg4510 transgenic mice. At 20 weeks of age in the control mouse cerebral cortex, there were 178.5 ± 66.2 microglia/mm$^2$ versus 444.2 ± 55.9 microglia/mm$^2$ in the rTg4510 mice ($P = 1.9 \times 10^{-3}$). In the control mouse hippocampus, there were 236.7 ± 17.7 microglia/mm$^2$ versus 471.0 ± 42.0 microglia/mm$^2$ in the rTg4510 mice ($P = 5.11 \times 10^{-3}$). Astrocytes labeled with GFAP antibody in (**I**) nontransgenic control and (**J**) transgenic mice at 20 weeks of age showed cortical astrogliosis accompanying MC1 immunoreactivity in the rTg4510 mice. Activated hypertrophied astrocytes are shown in the inset. (**K**) Percentage area in the coronal sections stained for GFAP was calculated. The cortical GFAP signal ($P = 9.14 \times 10^{-4}$, ANOVA) quantified in rTg4510 mice at 20 weeks of age increased compared to age-matched control mice ($P = 9.2 \times 10^{-3}$). The cortical GFAP signal also increased in 20-week-old transgenic mice compared to 5-week-old transgenic mice ($P = 0.020$). The hippocampal GFAP signal in transgenic and control mice at 5 and 20 weeks of age did not differ ($P = 0.676$, ANOVA). Statistics shown for Tukey's HSD (honestly significant difference) post hoc tests. Group sizes: $n = 3$ (female:male ratio; control 5 wk, 2:1; Tg 5 wk, 1:2; Ctr 20 wk, 1:2; Tg 20 wk, 2:1). Scale bars, 1 mm. *$P < 0.05$, **$P < 0.01$, and ***$P < 0.001$.

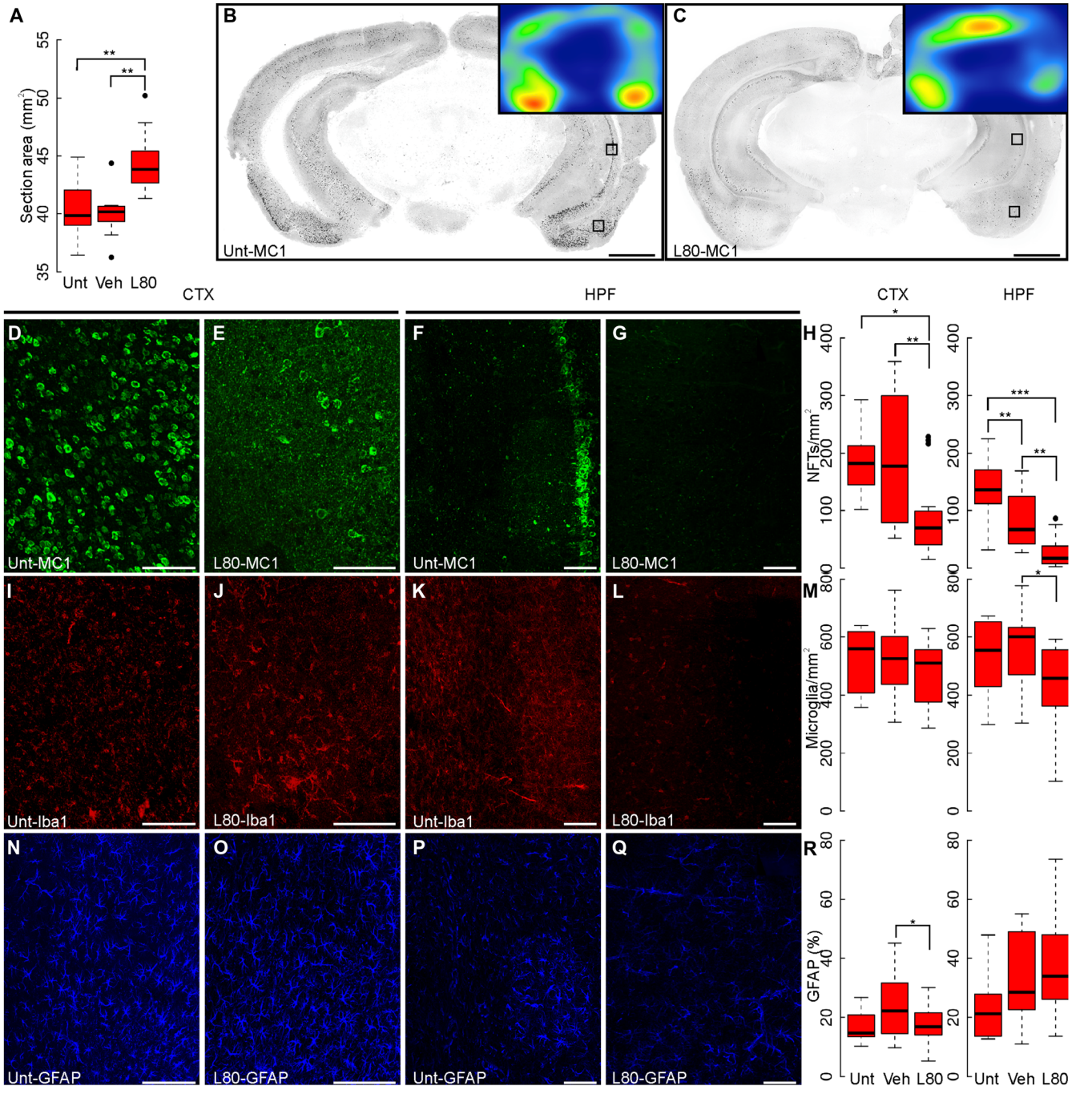


**Fig. 2. Lonafarnib treatment prevents neurofibrillary tangle formation and microgliosis.** (**A**) Brain coronal section area in 20-week-old rTg4510 transgenic mice that received chronic oral administration of lonafarnib (L80) versus untreated transgenic mice (Unt) or transgenic mice treated with vehicle alone (Veh). (**B** and **C**) Reduction of the extent of MC1 immunoreactivity in lonafarnib (L80)–treated transgenic mice compared to untreated mice. Scale bars, 1 mm. (**D** to **G**) Detail of insets of (B) and (C) showing representative MC1 immunoreactivity for the cortex (CTX) and hippocampus (HPF) of either untreated or lonafarnib-treated (L80) 20-week-old transgenic mice. (**H**) Large-scale coronal section mosaics quantified for MC1 immunoreactivity per square millimeter indicate a reduction of tau pathology after lonafarnib treatment (L80) when compared to untreated mice or animals treated with vehicle alone. (**I** to **L**) Density of microglia in the cortex and hippocampus of transgenic mice treated with lonafarnib (L80) or untreated is shown by Iba1 immunolabeling. Hippocampal microglial reactivity declined upon lonafarnib treatment. (**M**) Microglia quantification of coronal section mosaics in both the cortex and hippocampus of transgenic mice treated with lonafarnib. No statistically significant differences were observed in the cortex ($P = 0.667$, ANOVA) of lonafarnib-treated transgenic animals (489.16 ± 10.32 Iba1-positive cells/mm$^2$) when compared to vehicle-treated (520.35 ± 10.71 Iba1-positive cells/mm$^2$) or untreated animals (515.45 ± 11.03 Iba1-positive cells/mm$^2$). (**N** to **Q**) Astrocytes immunostained for GFAP in the cortex or hippocampus of untreated and lonafarnib-treated rTg4510 mice and (**R**) quantification of GFAP signal in full coronal slices. Neither lonafarnib (L80) nor vehicle alone altered astrocytes in 20-week-old transgenic mice in the hippocampus ($P = 0.236$, ANOVA), but a significant reduction was observed in the cortex when comparing lonafarnib-treated to vehicle-treated mice ($P = 0.042$). Statistics shown for Tukey's HSD post hoc tests. Group sizes: $n = 6$ (female:male ratio; Unt, 1:5; Veh, 3:3; L80, 3:3). Scale bars, 100 μm. *$P < 0.05$, **$P < 0.01$, and ***$P < 0.001$.

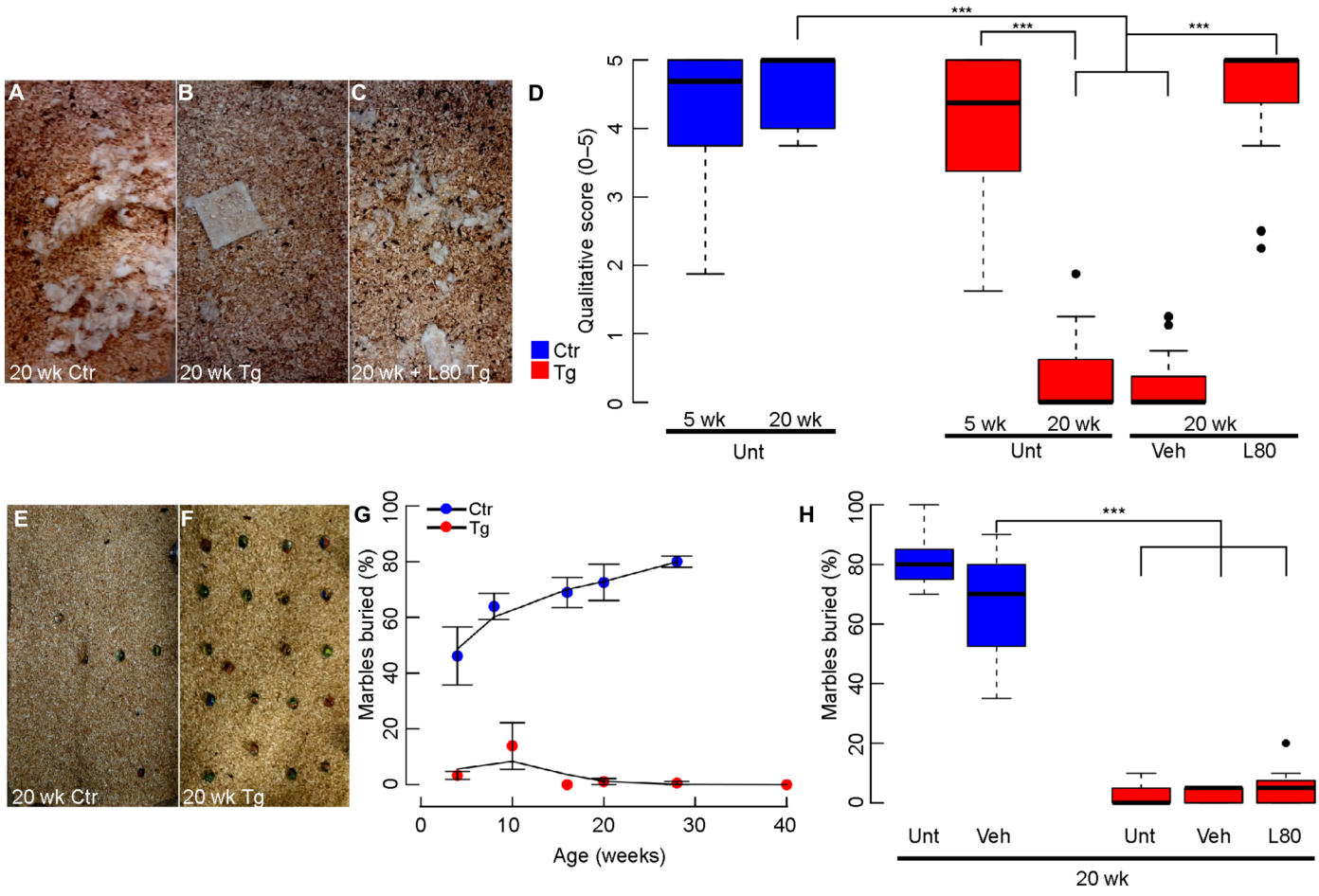


**Fig. 3. Chronic lonafarnib treatment ameliorates a nest building deficit in rTg4510 mice.** (**A**) At 20 weeks of age, littermate control mice display normal nest shredding behavior, but (**B**) transgenic animals failed to demonstrate nest shredding, as shown in the representative photographs. (**C**) Lonafarnib-treated 20-week-old rTg4510 animals shredded their nest. (**D**) Twenty-week-old transgenic mice had nest quality scores averaging 0.3 ± 0.1 in untreated mice or 0.2 ± 0.1 in mice treated with vehicle (Veh) alone, whereas the age-matched WT mouse nest shredding score averaged 3.7 ± 0.1 (both, $P < 5.3 \times 10^{-9}$). Chronic and intermittent oral administration of lonafarnib (L80) (80 mg/kg per day) rescued nest building, with nest scores averaging 3.5 ± 0.2 for treated mice. Qualitative scores were blindly assigned by observers using a scale from zero for untouched nesting material to five for a fully shredded nest ($n = 6$). (**E**) Twenty-week-old littermate control mice buried 80 ± 2.0% of the 20 marbles in 30 min, but (**F**) 20-week-old transgenic mice completely lacked digging behavior. (**G**) Control mice increased the percentage of marbles buried with age. They buried 40% of the marbles at 5 weeks of age and peaked at 30 weeks of age with an average of 80% of the marbles buried. Transgenic mice failed to bury marbles as early as 5 weeks of age {two-way ANOVA: genotype, $P < 2 \times 10^{-16}$; age, $P = 0.140$ [not significant (n.s.)]; interaction, $P = 1.93 \times 10^{-5}$}. (**H**) Marble burial deficits were rescued by neither lonafarnib (L80) nor vehicle treatment. Data are presented as box plots of percentage marbles buried per treatment group. Statistics shown for post hoc Wilcoxon tests. $n = 9$ (female:male ratio; Ctr Unt, 8:4; Tg Unt, 4:8; Tg Veh, 5:4; Tg L80, 4:5). ***$P < 0.001$.

remained unchanged, suggesting their accelerated clearance by lysosomes (Fig. 4, A to C, and fig. S4, A and B). Similar results were reproduced in neuroblastoma N2a cells (fig. S4C). Macroautophagy up-regulation by lonafarnib was confirmed using immunoblotting to quantify flux of LC3 and the autophagy receptor p62 in both cell types (fig. S5). Lonafarnib-treated rTg4510 mice also displayed changes in these two autophagy-related proteins compatible with increased macroautophagy in brain lysates (fig. S5, C to E). The accumulation of p62 and a trend toward higher LC3-II protein observed in brain lysates from rTg4510 mice at 20 weeks of age were markedly reduced in the lonafarnib-treated rTg4510 mice to the point that these animals no longer differed significantly from control mice ($P = 0.1579$; fig. S5, C to E). The stimulatory effect of lonafarnib was preferentially on basal macroautophagy, as inferred by the fact that addition of lonafarnib to NIH3T3 mouse fibroblasts in which macroautophagy was induced either by paraquat or thapsigargin did not further increase macroautophagy flux (fig. S4D). To determine whether lonafarnib also stimulated other forms of autophagy and to confirm that the observed increase in macroautophagy was not a consequence of a blockage in another degradation pathway, we used a photoswitchable reporter for chaperone-mediated autophagy (CMA) (KFERQ-PS-Dendra) (Fig. 4D and fig. S4, E and F) *(8, 33)* and a KFERQ-split-Venus double reporter for endosomal autophagy (Fig. 4E) *(8, 34)*. Lonafarnib stimulated both forms of selective autophagy with maximal effect in the lower concentration range. In the case of CMA, the stimulatory effect of lonafarnib was more pronounced on basal CMA, but a significant increase was still observed after inducing CMA with paraquat or thapsigargin ($P = 0.041$ for paraquat and $P = 0.003$ for thapsigargin; fig. S4, E and F). Inhibition of lysosomal proteolysis with $NH_4Cl$ and leupeptin in NIH3T3 cells expressing the KFERQ-split-Venus

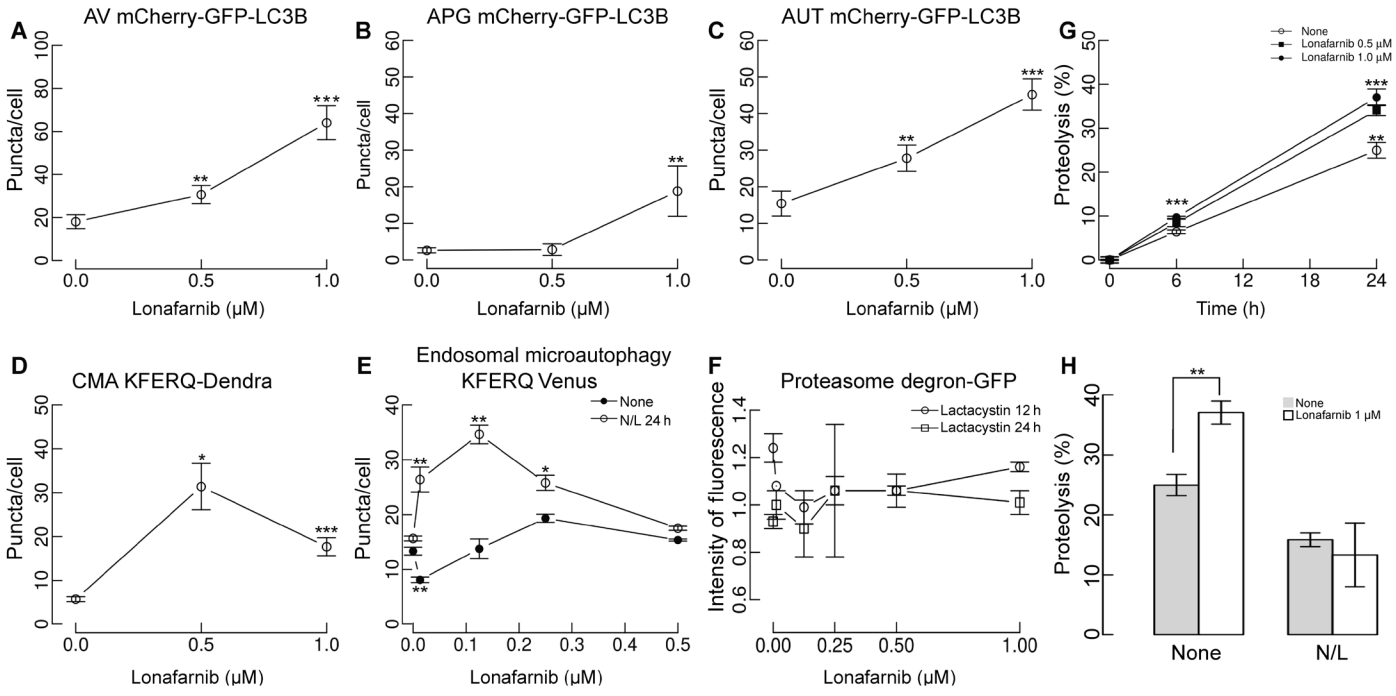


**Fig. 4. Inhibition of farnesyltransferase activates autophagy.** (**A** to **C**) NIH3T3 cells expressing the tandem reporter mCherry-GFP-LC3B were exposed to the indicated concentrations of lonafarnib for 48 hours. The quantified number of autophagic vacuoles (AV), autophagosomes (APG), and autolysosomes (AUT) is shown. (**D**) NIH3T3 cells expressing the KFERQ-Dendra reporter were photoswitched and treated with lonafarnib as indicated above. CMA was quantified by the number of fluorescent puncta positive for the photoconverted Dendra per cell. (**E**) NIH3T3 cells expressing N- and C-terminal KFERQ-split-Venus and treated with lonafarnib for 48 hours either were treated with 20 mM $NH_4Cl$ and 100 μM leupeptin (N/L) or were left untreated for the last 24 hours to quantify the effect of lonafarnib on targeting (None) and degradation (N/L) by endosomal microautophagy. Quantifications in (A) to (G) were done in at least 2500 cells per condition in three different experiments using high-content microscopy. (**F**) Results for NIH3T3 cells expressing degron-GFP and treated with lonafarnib for 48 hours and supplemented with 100 μM lactacystin for the last 12 or 24 hours. Proteasome-dependent degradation was calculated as the increase in the intensity of fluorescence upon lactacystin addition and after discounting the increase observed in cells treated under the same conditions but expressing a nonubiquitinable degron-GFP mutant. Values are expressed relative to the proteasome degradation in cells not treated with lonafarnib that were given an arbitrary value of one. (**G**) Total rates of intracellular protein degradation measured in NIH3T3 cells labeled with [$^3$H]leucine for 48 hours. The rate of proteolysis was calculated as the percentage of the initial acid-precipitable radioactivity (proteins) transformed into acid-soluble radioactivity (amino acids and small peptides) at the indicated times. (**H**) The contribution of lysosomes to total protein degradation was analyzed by supplementing cells with $NH_4Cl$ and leupeptin. Data are presented as means ± SEM ($n$ = 6 wells in three independent experiments). *$P$ < 0.05, **$P$ < 0.01, and ***$P$ < 0.001.

reporter demonstrated that lonafarnib not only promoted more efficient delivery of substrate to late endosome/multivesicular bodies via endosomal microautophagy but also stimulated efficient internalization and degradation in this compartment (Fig. 4E). Lonafarnib had no measurable effect on proteasome-dependent degradation monitored in the same cell type using a degron-GFP reporter (Fig. 4F) *(35)*.

The overall effect in all types of autophagy suggested a direct effect of lonafarnib in endosomal/lysosomal compartments shared by all of these autophagic pathways without influencing the proteasome. To assess this possibility, we evaluated proteolysis of long–half-life proteins after labeling newly synthesized proteins with [$^3$H]leucine for a 48-hour pulse. Lonafarnib increased proteolysis in a dose-dependent manner (Fig. 4G), an effect that was abolished in the presence of $NH_4Cl$ and leupeptin (Fig. 4H). These data support the idea that lonafarnib treatment resulted in an overall improvement in lysosomal function and the pathways that mediate delivery of cargo to this compartment.

## Rhes inhibition can reduce tau-related pathology

We sought the relevant targets of farnesyltransferase inhibition that could account for the ameliorative effects of lonafarnib on tau pathology in rTg4510 mice. Ras family members are among the prominent substrates of farnesyltransferase, and this modification is required for their correct localization at the inner surface of the plasma membrane and for their biological activity. Of particular interest was the Ras family member, Rhes, because it is prenylated by farnesyltransferase *(14)*, activates autophagy, and can modulate the aggregation state of mHtt by promoting its sumoylation *(18)*. To demonstrate that the effect of lonafarnib on tau pathology in rTg4510 mice could, in part, be accounted for by the inhibition of Rhes farnesylation, we modulated Rhes directly. Adeno-associated viral vectors (AAVs) carrying Rhes for overexpression or Rhes small interfering RNA (siRNA) for silencing were injected into the right entorhinal cortex of 10-week-old rTg4510 mice. When analyzed at 20 weeks of age (Fig. 5, A to F), silencing of Rhes using a microRNA backbone (Rhes-miR) markedly reduced the number of MC1-positive neurons (cortex: $P = 3.99 \times 10^{-4}$, hippocampus: $P = 3.61 \times 10^{-3}$; Fig. 5H), reduced microgliosis (cortex: $P = 1.50 \times 10^{-4}$, hippocampus: $P = 3.3 \times 10^{-4}$; Fig. 5I), and increased the coronal section area ($P = 0.002$; Fig. 5G). Therefore, Rhes inhibition recapitulated the effects of lonafarnib treatment. Rhes overexpression did not appear to worsen tau pathology (Fig. 5).

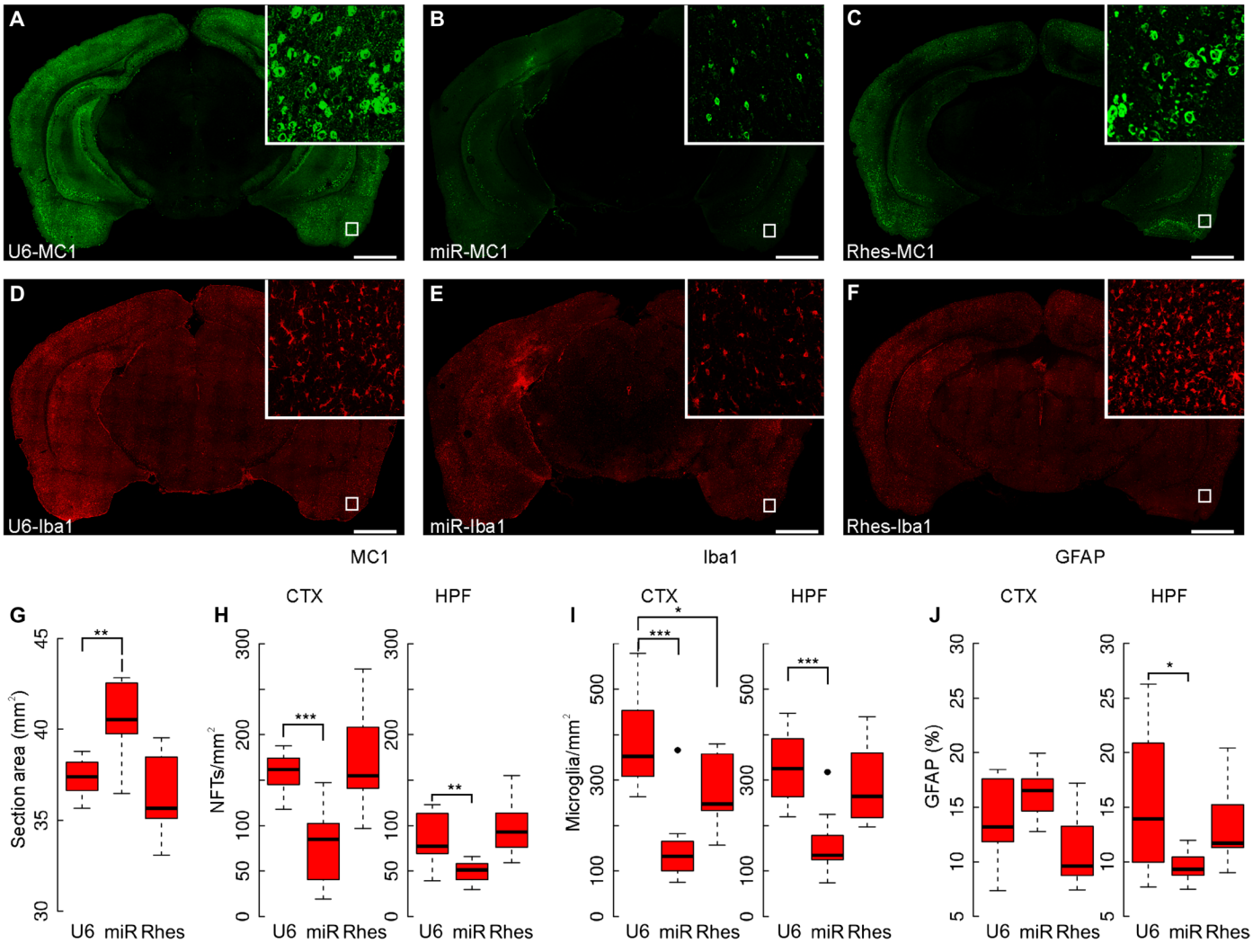


**Fig. 5. Rhes suppression mimics the protective effect of lonafarnib in rTg4510 mice.** Ten-week-old transgenic rTg4510 mice were intracranially infected with AAV 2/5 containing either U6, Rhes-miR, or Rhes-WT constructs and were sacrificed at 20 weeks of age. (**A** to **C**) Full mosaic immunohistochemistry for MC1 immunoreactivity after Rhes suppression by Rhes-miR showed fewer neurofibrillary tangles than did transduction with U6 or Rhes-WT. (**D** to **F**) Full mosaic immunohistochemistry for Iba1 was also reduced in mice treated with Rhes-miR. The quantification of micrographs indicates (**G**) significantly increased coronal section area for Rhes-miR (40.53 ± 0.70 $mm^2$; $P = 0.002$) but not Rhes-WT (36.41 ± 0.79 $mm^2$; $P = 0.307$) in injected transgenic mice compared to U6 (37.33 ± 0.36 $mm^2$). (**H**) There were a reduced number of MC1-positive cells per square millimeter both in the cerebral cortex (CTX) and hippocampus (HPF). The cortical density of MC1-positive cells per square millimeter in animals injected with U6 was 157.81 ± 12.56 compared to Rhes-miR (78.76 ± 8.88 MC1-positive cells/$mm^2$; $P = 3.90 \times 10^{-4}$) or Rhes overexpression (172.15 ± 13.12 MC1-positive cells/$mm^2$; $P = 0.487$). In the hippocampus, injected mice had 86.09 ± 9.28 MC1-positive cells/$mm^2$ compared to Rhes-miR (49.15 ± 7.01 MC1-positive cells/$mm^2$; $P = 3.61 \times 10^{-3}$) or Rhes overexpression (92.86 ± 9.64 MC1-positive cells/$mm^2$; $P = 0.635$). (**I**) Rhes-miR reduced the number of microglia per square millimeter in the cortex and hippocampus in Rhes-miR–injected rTg4510 mice. Rhes-miR–injected transgenic mice showed a significant reduction in the cortex (compared to U6 control; $P = 1.50 \times 10^{-4}$) and hippocampus (compared to U6 control; $P = 3.02 \times 10^{-4}$), whereas Rhes-WT showed a reduction in the cortex ($P = 0.027$) with no effect observed in the hippocampus ($P = 0.531$). (**J**) No significant change was observed in astrocytic immunoreactivity in the cerebral cortex for either Rhes-miR ($P = 0.182$) or Rhes-WT overexpression ($P = 0.094$) compared to U6 controls. In the hippocampus, Rhes-miR significantly reduced GFAP immunostaining compared to U6 controls ($P = 0.029$) but not when compared to Rhes-WT overexpression ($P = 0.343$). $n = 3$ (female:male ratio; U6, 0:3; Rhes-miR, 0:3; Rhes, 3:0). Scale bars, 1 mm. *$P < 0.05$, **$P < 0.01$, and ***$P < 0.001$.

## Farnesyltransferase inhibition and Rhes suppression reduce global sumoylation and ubiquitination

We examined the effects of lonafarnib treatment or Rhes suppression upon sumoylation and ubiquitination in rTg4510 mice. These protein modifications are prominent features of tau pathology, and tau can undergo both modifications *(34, 36, 37)*. Lonafarnib administration significantly altered the number of cells with detectable sumoylation ($P = 0.002$; fig. S6, A to D and I) and ubiquitination ($P = 0.048$; fig. S6, E to H and L). Using the number of double- and single-labeled cells, we computed Bayesian probabilities for cells labeled by MC1, given that they were labeled with anti-sumo (fig. S6J) or anti-ubiquitin (fig. S6M). rTg4510 mice showed many sumo- and ubiquitin-positive cells without MC1 immunoreactivity (fig. S6, J and M). However, when using MC1 immunoreactivity as a prior, most MC1-positive cells were also labeled with sumo or ubiquitin (fig. S6, K and N). Treatment with lonafarnib significantly altered these probabilities of MC1-positive

labeling given sumoylation ($P = 2.71 \times 10^{-5}$; fig. S6J) or ubiquitination ($P = 0.016$; fig. S6M). The effects of lonafarnib on ubiquitin immunostaining were successfully replicated in total protein lysates from the cortex of treated rTg4510 mice (fig. S6, Q and R). However, because of the high variability of sumo measurements, densitometric analyses did not achieve statistical significance (fig. S6P). Rhes silencing similarly affected sumoylation but not ubiquitination (fig. S6, A, B, and I; $P = 0.047$ and fig. S6, E, F, and L; $P = 0.4033$). Treatment with Rhes-miR did not significantly reduce the double labeling of MC1-positive cells that were positive for sumo ($P = 0.063$; fig. S6J) but reduced those that were positive for ubiquitin ($P = 0.007$; fig. S6M).

### Linking lonafarnib treatment to Rhes-mediated effects on tau pathology

To link Rhes-induced tau pathology to Rhes farnesylation, we cultured mouse hippocampal neurons for 3 weeks, at which time we transduced an AAV (serotype 2/5) expressing Rhes, a GTPase-inactive Rhes mutant (Rhes S33N), or a microRNA to silence Rhes (Rhes-miR). As expected, Rhes overexpression markedly increased PHF-1 immunoreactivity (Fig. 6, A and B). Because the Rhes GTPase mutant increased PHF-1 tau and the Rhes-WT (Fig. 6A), we focused on Rhes as a substrate for prenylation by farnesyltransferase *(38)*. The farnesyltransferase inhibitor lonafarnib, when added to the culture medium, prevented PHF-1 tau accumulation in the presence of Rhes overexpression in a dose-dependent manner. A four-parameter log-logistic modeling (R package, drc) was statistically significant for each parameter estimated and provided the parameters for calculating an $IC_{50}$ (median inhibitory concentration) of 61.00 nM (Fig. 6, C and D).

We asked whether lonafarnib prevented PHF-1 tau accumulation, at least in part, by promoting degradation of Rhes through autophagic pathways. By overexpressing mCherry-Rhes in HeLa cells, we validated that lonafarnib was effective in reducing both total Rhes and the membrane-like Rhes fraction (fig. S7). However, inhibition of lysosomal proteolysis (with $NH_4Cl$/leupeptin) or macroautophagy (with 3MA) did not support lysosomal degradation of Rhes in the presence of increasing lonafarnib concentrations (fig. S8).

To determine whether the profile of proteostasis stimulation observed for lonafarnib paralleled its effects in hippocampal primary mouse neurons, 3-week-old cultures were transduced to overexpress Rhes in the presence of 250 nM lonafarnib and then were treated with either $NH_4Cl$/leupeptin, a lysosome inhibitor, or MG-132, a proteasome inhibitor. As predicted, the proteasome inhibitor MG-132 had no effect on the reduction of Rhes-mediated PHF-1 accumulation in the presence of lonafarnib (Fig. 6E). In contrast, lysosomal inhibition with $NH_4Cl$ and leupeptin was effective in blocking lonafarnib action, as observed by the steady accumulation of PHF-1 immunoreactivity (Fig. 6, E to G). p62 served as a positive control because it is known to undergo lysosomal degradation (Fig. 6H).

### Selective effects of lonafarnib on phospho-tau accumulation

Lonafarnib administration in rTg4510 mice specifically reduced pathological tau as detected by Western blot with antibodies against PHF-1, MC1, AT8, and AT100 in mouse cortical protein lysates, without a significant effect on total tau, as detected with TAU5 antibody (lonafarnib-treated versus untreated, $P = 0.600$; lonafarnib-treated versus vehicle, $P = 0.999$; Fig. 6, I to N). In addition, sarkosyl-insoluble high–molecular weight tau observed in vehicle-treated aged rTg4510 mice was not present in aged mice treated with lonafarnib (Fig. 6O). Lonafarnib treatment also reduced phospho-tau in human induced pluripotent stem cell (hiPSC)–derived neurons, which was readily detectable in these cells using an enzyme-linked immunosorbent assay (ELISA) specific for human phospho-tau $Thr^{181}$. hiPSC-derived neurons expressing either *MAPT*-WT or *MAPT*-R406W were cultured for 4 weeks and then treated with either dimethyl sulfoxide (DMSO) or 10 μM lonafarnib for an additional 9 days. Intracellular phospho-tau was significantly reduced by lonafarnib treatment (fig. S9A, $P = 0.02$, and fig. S9B, $P = 0.03$). Phospho-tau was also elevated in hiPSC-derived neurons carrying the pathogenic *MAPT*-P301L mutation ($P = 1 \times 10^{-4}$; fig. S9C), despite the caveat that these cells were insufficiently mature to express 4R tau abundantly. hiPSC-derived neuron protein lysates treated with λ-phosphatase and then blotted with E3T antibody, which is specific for tau 4R isoforms, demonstrated expression of the alternatively spliced tau exon (fig. S9D).

### Rhes expression during development homeostatically regulates tau

hiPSC-derived neurons were obtained from patients with frontotemporal dementia harboring the *MAPT* mutations P301L *(39)*, G55R *(40)*, V337M *(41)*, R406W *(42)*, or *C9ORF72* expansion *(43)*. hiPSC-derived neurons from patients and from clinically healthy age-matched controls were analyzed by RNA sequencing (RNAseq) (Fig. 7A). Three genes were differentially expressed with the same sign in their log fold change (log FC) for every *MAPT* mutation hiPSC cell line, but were not differentially expressed in the C9ORF72 (chromosome 9 open reading frame 72) line or in any control lines (Fig. 7B; fig. S10, D and E; and data file S1). One of the three genes was *RASD2*, which encodes Rhes (Fig. 7B). The other two genes were the serine-threonine kinase, *NEK9* (fig. S10D), and the zinc finger protein, *ZFP41* (fig. S10E). The neuronal markers *MAPT*, which encodes tau (Fig. 7C), and *TUBB3*, which encodes pan-neuronal β-tubulin (Fig. 7D), were not differentially expressed among neurons from patients carrying tau mutations. The DE genes were validated by digital reverse transcription polymerase chain reaction (RT-PCR) quantification for their expression in total RNA samples taken from each of the hiPSC-derived neuronal lines at 5 weeks using *GAPDH* (glyceraldehyde-3-phosphate dehydrogenase) as internal control (Fig. 7, E to G, and fig. S10, F and G). Further statistical validation was obtained by bootstrapping ANOVA tests ($k = 1000$) of their expression counts per million (CPM) [bootstrapped *P* values: *RASD2*, $P = 8 \times 10^{-3}$; *ZFP41*, $P = 0.047$; *NEK9*, $P = 0.348$ (n.s.)] *(44)*. Differential expression of *RASD2* in tau mutant hiPSC-derived neurons was confirmed in a set of isogenic control cell lines. Real-time RT-PCR in three independent sets of hiPSC-derived neurons with different MAPT mutations and their isogenic control counterparts showed the expected differential expression of *RASD2* (*MAPT*-P301L/P301S, Fig. 7H; *MAPT*-V337M, Fig. 7I; and *MAPT*-R406W, Fig. 7J). In agreement with the RNAseq data, *MAPT* expression did not change significantly in any of the isogenic control cell lines ($P = 0.514$, ANOVA, Fig. 7K; $P = 0.4019$, Welch *t*-test, Fig. 7L; $P = 0.4334$, Welch *t*-test, Fig. 7M)

*RASD2* expression was decreased in the hiPSC-derived neurons from frontotemporal patients carrying tau mutations relative to the neurons from healthy person controls. As these neurons differentiated, *RASD2* expression increased in the control line; however, in *MAPT-P301L* and *MAPT-V337M* lines, *RASD2* remained low throughout differentiation (Fig. 8A). Over this same time period, *MAPT* expression increased and showed no statistical difference between cells with and without tau mutations (Fig. 8B). Thus, under control conditions, *RASD2* expression rose coincident with increased tau, but this

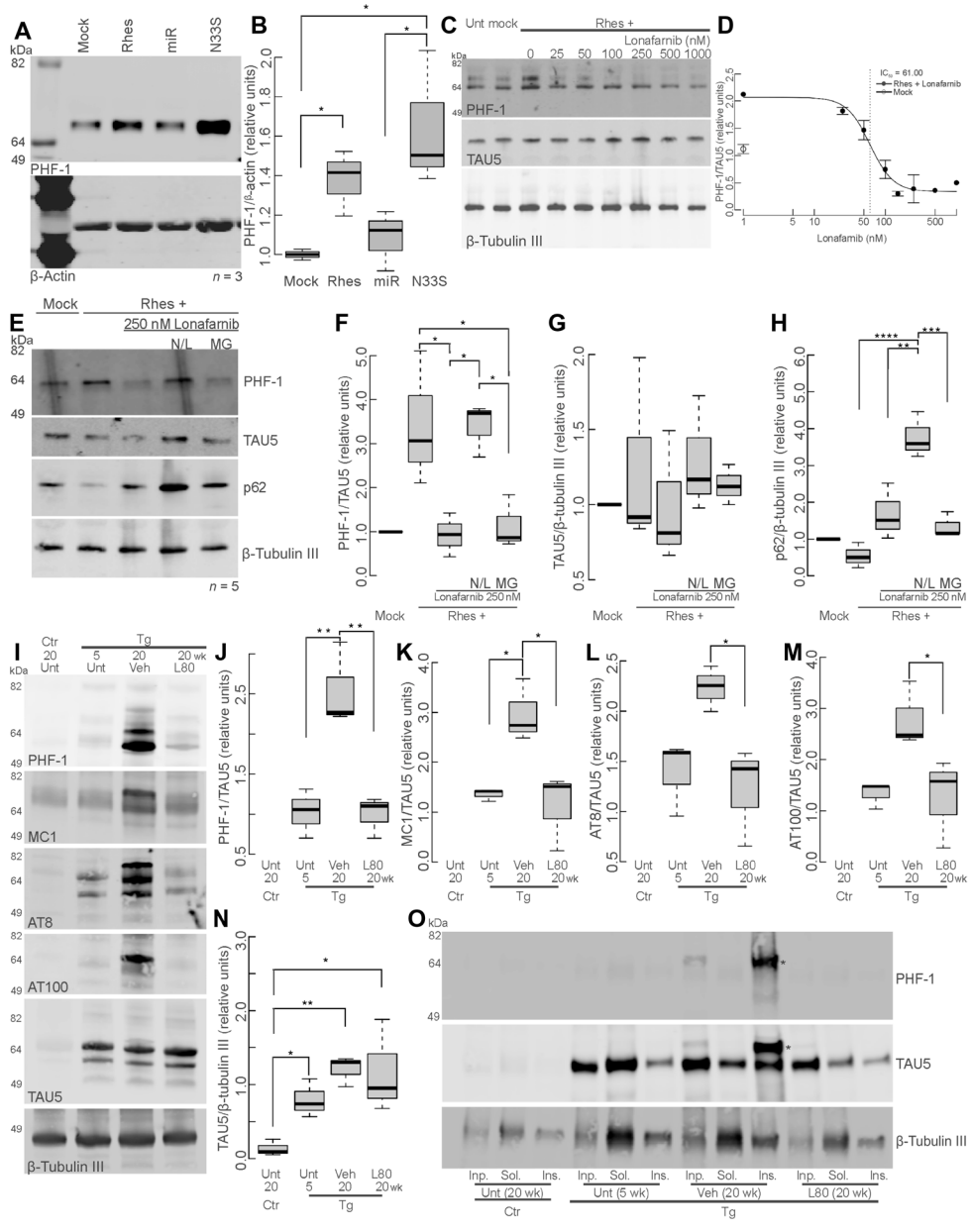


**Fig. 6. Farnesyltransferase inhibition prevents Rhes-mediated tau accumulation and activates autophagy.** (**A**) Overexpression of either Rhes-WT or the GTPase-inactive mutant Rhes-S33N but not Rhes silenced by microRNA (Rhes-miR) in hippocampal primary mouse neurons increased PHF-1 phospho-tau. Representative blot (A) and densitometry quantification (**B**) of independent replicates. (**C**) Farnesyltransferase inhibition with lonafarnib rescued the Rhes-induced increase in phosphorylated tau in a dose-dependent manner. Representative blot (C) and densitometry quantification (**D**) of independent replicates. β-Actin was used for a loading and normalization control. A four-parameter log-logistic model fit (R package, drc) is shown [(B) $P = 0.006$; (C) $P = 0.010$; (D) $P < 1 \times 10^{-4}$, $IC_{50} = 61.00$ nM, $P < 1 \times 10^{-4}$]. (**E** to **H**) Primary mouse neuronal cultures (Mock) were transduced with AAV 2/5 to overexpress Rhes and then were either left untreated (Rhes-positive), treated with 250 nM lonafarnib alone (Lon), or additionally treated either with a cocktail containing 20 mM $NH_4Cl$ and 100 μM leupeptin (N/L) to block lysosomal-mediated proteolysis or with 5 μM MG-132 (*N*-carbobenzyloxy-L-leucyl-L-leucyl-L-leucinal) (MG) to block proteasome activity. Cell lysates were obtained at 12 hours, or cell media and inhibitors were replenished at 12 hours and lysates were collected at 24 hours, as indicated. (E) Proteins in the cell lysates were separated by SDS–polyacrylamide gel electrophoresis (SDS-PAGE) and then Western-blotted for PHF-1 S496/phospho-tau, total tau (TAU5), and p62. (F) PHF-1 antibody was normalized to TAU5; (G) TAU5 or (H) p62 was normalized to β-tubulin III and plotted as means ± SEM. Lonafarnib prevented a Rhes-mediated PHF-1 increase, an effect reversed by lysosomal proteolysis inhibition (N/L) but not by proteasome inhibition (MG). (**I**) Western blot of cortical lysates from untreated rTg4510 mice at 20 weeks of age (Ctr), untreated (Unt) transgenic mice at 5 weeks of age, and either vehicle (Veh) or lonafarnib-treated transgenic mice at 20 weeks of age. Western blots (I) were treated with antibodies to pathological tau, total tau (TAU5), and β-tubulin III as the loading control; (**J** to **N**) their respective densitometric quantifications are presented. Phosphorylated and conformational tau were normalized to TAU5, and TAU5 was normalized to β-tubulin III ($n = 3$). (**O**) Sarkosyl-insoluble tau fractions were isolated from mouse cortical lysates; a 64-kDa apparent high–molecular weight tau band is indicated by the asterisk in cortical lysates from aged rTg4510 mice, but no comparable band was detectable in control, young, or age-matched lonafarnib-treated rTg4510 mice. (A and B and I to N) $n = 3$. (I to N) Female:male ratio; Unt Ctr 20 wk, 0:3; Unt Tg 5 wk, 1:2; Veh Tg 20 wk, 1:2; L80 Tg 20 wk, 2:1. (C and D and E to H) $N = 5$ independent experiments. Statistical analysis: one-way ANOVA and Tukey's HSD post hoc tests.*$P < 0.05$, **$P < 0.01$, ***$P < 0.001$, and ****$P < 1 \times 10^{-4}$.

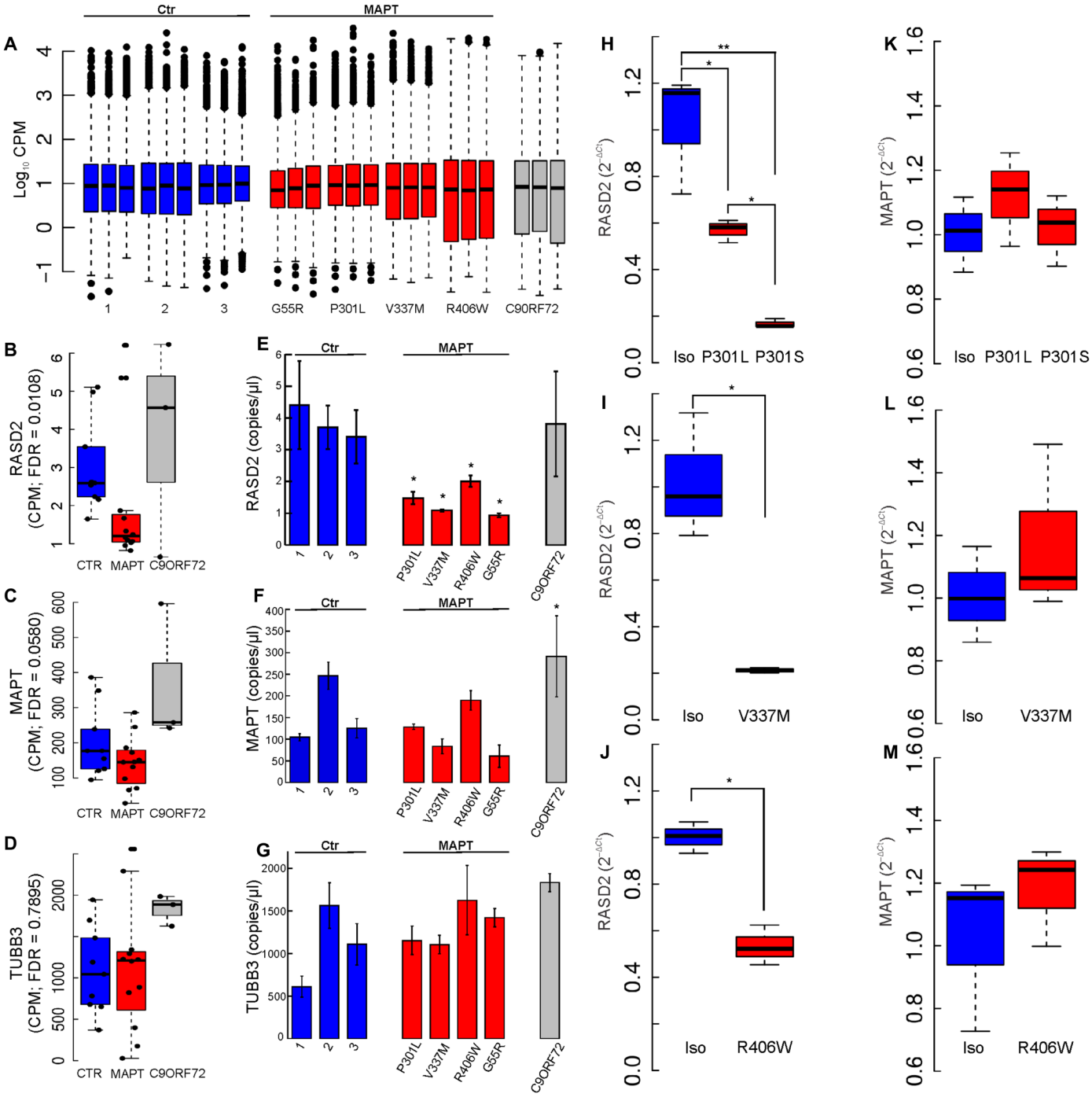


**Fig. 7. RASD2 expression is reduced in transcriptome profiles of hiPSC-derived neurons from patients with frontotemporal dementia carrying MAPT mutations.** (**A**) RNAseq of hiPSC-derived neurons from patients with frontotemporal dementia carrying *MAPT* mutations (G55R, P301L, V337M, and R406W) or a *C9ORF72* expansion versus three age-matched healthy controls cultured for 5 weeks. Box plots of normalized CPMs per library are shown. (**B**) RASD2 expression was deregulated across each patient line carrying *MAPT* mutations. FDR, false discovery rate. (**C**) *MAPT* expression did not change across iPSC-derived neurons with different *MAPT* mutations. (**D**) TUBB3 was highly expressed and remained unaltered across samples. Digital PCR data (**E** to **G**) presented as mean copies/µl ± SEM validated the findings of each of these genes for each cell line studied. RASD2 suppression in the presence of tau mutations in neurons differentiated from hiPSCs compared to their respective isogenic control lines was verified by TaqMan RT-PCR using (**H**) F0510 cells harboring P301L and P301S mutations ($P = 1.45 \times 10^{-3}$, ANOVA), (**I**) hiPSC-derived neurons harboring the MAPT-V337M mutation ($P = 0.035$, *t* test), and (**J**) hiPSC-derived neurons harboring the MAPT-R406W mutation ($P = 2.14 \times 10^{-3}$, *t* test). (**K** to **M**) *MAPT* expression remained unchanged in hiPSC-derived neurons carrying different *MAPT* mutations and in the corrected isogenic lines. *$P < 0.05$ and **$P < 0.01$.

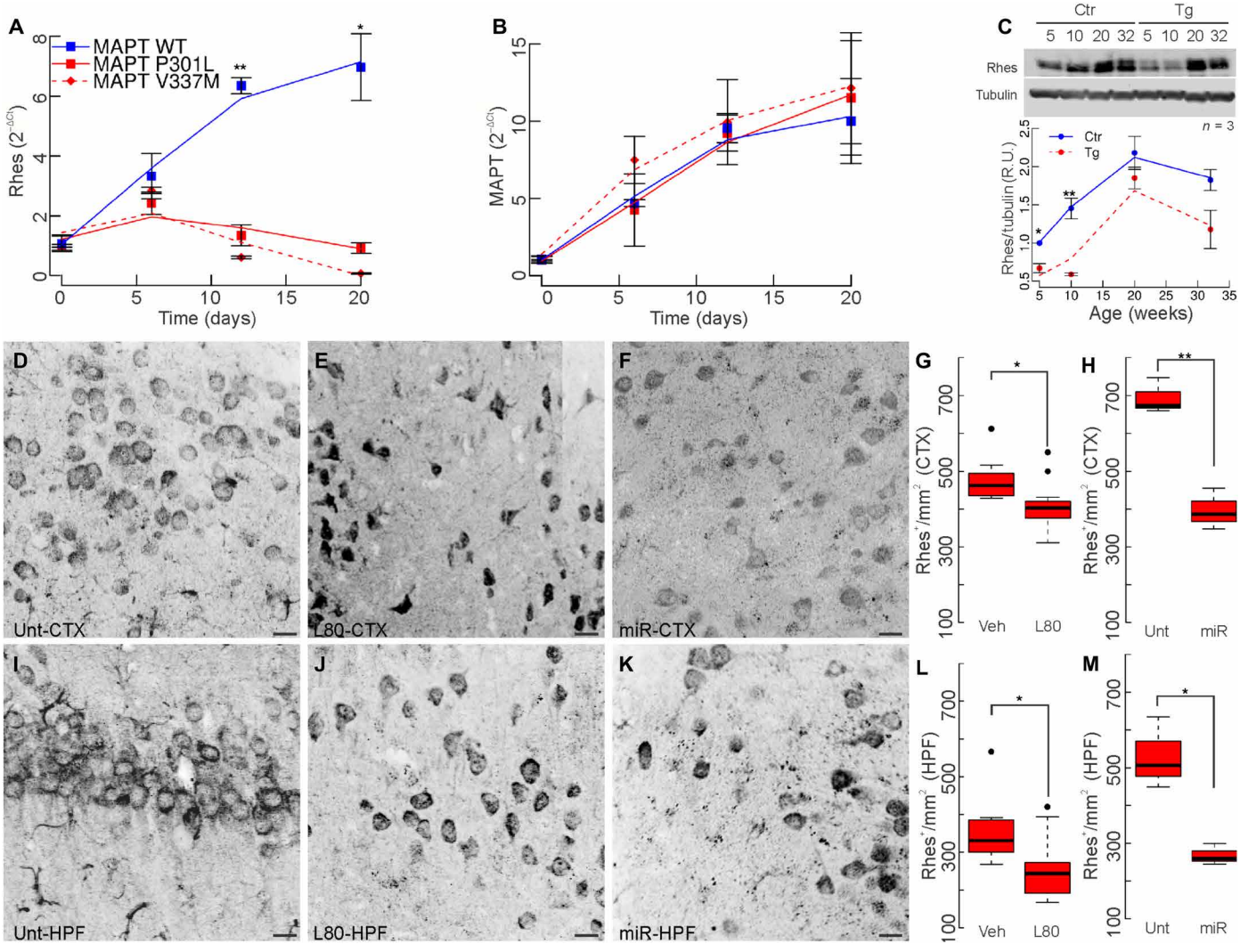


**Fig. 8. Rhes expression increases as neurons age, which can be prevented by tau mutations.** (**A**) Rhes expression is reduced in *MAPT*-P301L and *MAPT*-V337M hiPSC-derived neurons during hiPSC differentiation into neurons as early as the neurorosette stage; Rhes expression increases during differentiation into neurons of hiPSCs carrying *MAPT*-WT. (**B**) *MAPT* expression increases continuously during neuronal differentiation regardless of *MAPT* genotype. (**C**) Rhes quantification in the brains of rTg4510 transgenic mice and littermate controls. Rhes increases as both transgenic and control mice age, but these increases are significantly lower than for younger transgenic mice [two-way ANOVA: age, $P = 3.24 \times 10^{-3}$; genotype, $P = 8.01 \times 10^{-3}$; interaction, $P = 0.88$ (n.s.)]. (**D** to **M**) Rhes reduction in 20-week-old transgenic mice by both lonafarnib and Rhes-miR treatments. Untreated rTg4510 mice had a mean of 693.3 ± 27.0 Rhes-positive cells/mm$^2$ in the cortex (CTX) and 530.0 ± 54.9 cells/mm$^2$ in the hippocampus (HPF). Chronic administration of lonafarnib reduced Rhes to 409.1 ± 18.5 cells/mm$^2$ ($P = 5.62 \times 10^{-3}$) in the cortex and to 252.6 ± 23.7 cells/mm$^2$ ($P = 9.29 \times 10^{-3}$) in the hippocampus. Rhes-miR treatment reduced Rhes to 396.27 ± 31.52 cells/mm$^2$ ($P = 0.002$) in the cortex and to 268.1 ± 16.1 cells/mm$^2$ ($P = 0.033$) in the hippocampus. Statistics shown for Wilcoxon tests. (A to C) $n = 3$ (female:male ratio; Ctrs 5 wk 1:2, 10 wk 0:3, 20 wk 2:1, 32 wk 2:1; Tg 5 wk 3:0, 10 wk 0:3, 20 wk 2:1, 32 wk 1:2). (D to M) $n = 3$ (female:male ratio; Unt, 0:3; L80, 3:3; Veh, 3:3; Rhes-miR, 1:2). Scale bars, 100 μm. *$P < 0.05$ and **$P < 0.01$.

physiological increase was suppressed in the presence of tau mutations. Because iPSC-derived neurons remained relatively immature, tracking *RASD2* at more advanced ages was not possible. Therefore, the *RASD2* transcript was measured in rTg4510 transgenic mouse *(24)* brains and those of their littermate controls at 5, 10, 20, and 32 weeks. Consistent with cultured cell line results, as mice aged, Rhes increased (Fig. 8C). Rhes expression was lower in younger transgenic mice (5 and 10 weeks of age) that expressed mutant tau than their littermate controls that expressed only WT mouse tau. However, by 20 and 32 weeks of age, the difference between transgenic mice and littermate controls was no longer significant. These observations suggested that a compensatory Rhes reduction could protect younger animals by maintaining lower Rhes expression. Lonafarnib-mediated lowering of Rhes expression, as observed in the animal experiments, replicated the early homeostatic response to tau mutations in the rTg4510 mouse cortex (Fig. 8, D to H) and hippocampus (Fig. 8, I to M).

## DISCUSSION

Attempts to treat the genetic tauopathies have been impeded by the absence of an understanding of the molecular pathways that connect

genotype to phenotype. The effects of the farnesyltransferase inhibitor lonafarnib on tau pathology allowed this drug to serve as a probe for the discovery of disease-relevant pathways. Although farnesyltransferase inhibitors, such as lonafarnib, affect many farnesylated substrates, the major effects of the drug appear to be mediated through membrane-associated Rhes. Therefore, the data point to this regulated pathway as a druggable target for tauopathies and possibly other neurodegenerative diseases where pathological inclusions are mediated by lysosomal dysfunction. Lonafarnib had its principal effect on enhancing protein degradation in the lysosome (Fig. 4). When Rhes was overexpressed in mouse primary neurons to increase PHF-1 and the neurons were then treated with lonafarnib, the effects of the drug on PHF-1 were prevented by the lysosomal inhibitors $NH_4Cl$ and leupeptin (Fig. 6, E to H). Furthermore, inhibition of Rhes in the rTg4510 mouse phenocopied the effects of lonafarnib (Fig. 5). Positing the lysosome as the drug target in the mouse is consistent with observations that the P301L tau mutation interferes with the degradation of tau through all autophagic pathways *(8)*.

Contributing to the mechanism of Rhes action is its role as a sumo ligase *(18)*. Tau is both sumoylated *(36)* and ubiquitinated *(37, 45)*. However, in contrast to mHtt, which was reported to bind to Rhes *(18)*, we did not observe an interaction between Rhes and tau in coimmunoprecipitates of rTg4510 cortical lysates (fig. S11). Both Rhes-miR and lonafarnib were able to suppress sumoylation and ubiquitination in rTg4510 mice (fig. S6). We observed some sumo- and ubiquitin-positive cells in the absence of MC1 immunoreactivity, suggesting the presence of substrates other than tau for these proteins (fig. S6, K and N). Both lonafarnib and Rhes-miR decreased the probabilities of double labeling, thereby suggesting a link between the Rhes pathway and activation of sumoylation and ubiquitination (fig. S6). However, we could not observe changes in tau sumoylation or tau ubiquitination in the brain cortex of lonafarnib-treated mice (fig. S11), which could imply that sumo or ubiquitin targets, other than tau, are sensitive to this treatment and their identification warrants further investigation.

Many questions remain regarding the pathway, from membrane disassociation of Rhes to lysosomal activation (fig. S12). Farnesylation of Rhes may serve as a switch between its effect on mTOR to inhibit autophagy and on beclin-Bcl2 to activate autophagy. The regulation of autophagy by Rhes under neurodegenerative disease conditions was reported to be independent of mTOR *(17)*; hence, strategies that activate mTOR may not be opportune therapeutic options. On the other hand, strategies that activate autophagy have shown beneficial effects *(10, 46)*. One limitation of our study is the broad effect of farnesyltransferase inhibition on many farnesylated proteins in cells besides Rhes. Whereas these broad effects of farnesyltransferase inhibition do not appear to be toxic, how they contribute to our findings will require further study.

From stem cells *(47)* to aged cells *(48)*, proteostasis is a highly regulated process over the lifespan. Rhes is developmentally regulated, being low in neuronal precursor cells and young animals and gradually increasing with maturation (Fig. 8). The persistently reduced Rhes in iPSC-derived neurons harboring tau mutations (Fig. 7) suggested a homeostatic response to the mutation *(17, 49)* by which the cell can sense tau mutations before inclusions are evident and respond by activating the lysosome through endogenous reduction of Rhes. An increase in lysosomal proteolysis in response to mutant tau expression has been reported *(8)*. Immature hiPSC-derived neurons and young rTg4510 mice appeared to compensate for the deleterious effects of the tau mutation by reducing Rhes (Figs. 7 and 8). Under control conditions, the *RASD2* transcript expression increased coincident with increases in tau, whereas this rise in Rhes failed to occur in the presence of tau mutations (Fig. 8, A and B). Tracking Rhes in hiPSC-derived neurons was limited by the fact that these cells do not fully mature. However, as tau pathology in rTg4510 mice advanced, cells escaped from the autoregulatory controls that lower Rhes to protect the cell, resulting in an increase in Rhes (Fig. 8C). This Rhes sensor system appeared to be sufficiently sensitive to detect the tau P301L mutation in the alternatively spliced tau exon 10, although its expression was low in hiPSC-derived neurons (fig. S9D). A similarly complex picture regarding the role of Rhes in HD and Parkinson's disease has been proposed *(17, 50)*. Rhes is down-regulated in these diseases *(50–52)*, yet in HD, increasing Rhes expression augments cytotoxicity *(39)*. Thus, the Rhes pathway serves as a highly sensitive sensor. By inhibiting Rhes farnesylation, Rhes is reduced probably because of its degradation when released from cell membranes.

The pharmacological approach described here will likely require early and chronic intervention. Once tau pathology emerged, lonafarnib was no longer effective. Nevertheless, the broad implication of proteostasis in many neurodegenerative diseases including Parkinson's disease, HD, Alzheimer's disease, and frontotemporal dementia *(48, 53, 54)* requires a concerted effort to explore relevant pathways for therapeutic effects. The safety profile of lonafarnib *(21, 22)* makes this drug a promising candidate for repurposing to treat tauopathies due to tau mutations.

## MATERIALS AND METHODS

### Study design

Using tau transgenic rTg4510 mice, we evaluated the effects of farnesyltransferase inhibition on one of its substrates, Rhes. The farnesyltransferase inhibitor lonafarnib and siRNA-mediated suppression were used to assess tau pathology and related behaviors in the mice. The study design included quantitative immunohistochemistry on mouse brain tissue for markers of tau pathology as well as behavioral testing such as marble burial, nesting, and circling. Mice were randomly assigned to experimental groups, and behavioral testing was documented by blinded investigators. Using primary cultures of hippocampal neurons from mice, we tested the effects of lonafarnib on phospho-tau. We determined the mechanism of lonafarnib action as an effector of tau protein degradation by probing autophagic/lysosomal and proteasome pathways in cell lines. Last, we used human neurons generated from iPSCs derived from patients with frontotemporal dementia harboring MAPT mutations to search for differential gene expression associated with the tau mutations.

### Animal studies

This study was conducted in accordance with the National Institutes of Health *Guide for the Care and Use of Laboratory Animals* and the Association and Accreditation of Laboratory Animal Care International guidelines and under the authorization of the Institutional Animal Care and Use Committee and the University of California, Santa Barbara. Animals were placed on a standard rodent diet ad libitum and housed under a 12-hour/12-hour light-dark cycle.

Transgenic rTg4510 mice *(24)* were purchased from the Jackson Laboratory (Bar Harbor, ME) and maintained by breeding B6 *CaMKII-tTA* heterozygotes (003010) with FVB.tetO-MAPT-P301L

heterozygotes (015815). Weanlings were PCR-genotyped with DNA obtained from an oral swab (Puritan, Guilford, ME) using KAPA mouse genotyping kits for DNA extraction and amplification (Kapa Biosystems, Wilmington, MA), as suggested by the Jackson Laboratory (PCR primers used: forward, oIMR8746; tTA reverse, oIMR8747; tTA control forward, oIMR8744; tTA control reverse, oIMR874; *MAPT* forward, 14159; *MAPT* reverse, 14160; *MAPT* control forward, oIMR7338; *MAPT* control reverse, oIMR7339). Identified double transgenics were used in the experiments and reported here as transgenics; littermates identified as negative for both tTA and *MAPT-P301L* were used as nontransgenic controls, where indicated. Doxycycline was not used to turn off the expression of *MAPT*-P301L transgene in this study.

Lonafarnib was synthesized by Cayman Chemical Company (Ann Arbor, MI), certified 99.9% or higher purity by high-performance liquid chromatography, and stored lyophilized at −20°C. Lonafarnib (100×) was dissolved in DMSO heated to 95°C until the solution was clear and 12 mg/ml was resuspended in 20% (2-hydroxypropyl)-β-cyclodextrin (Sigma-Aldrich) as a vehicle. Resuspended solution was stored at 4°C for less than a week. Ten-week-old rTg4510 mice were orally administered lonafarnib (80 mg/kg per day) or vehicle alone by gavage feeding in an alternate schedule of five consecutive days followed by five resting days for 10 weeks. Cortical protein lysates were blotted with HDJ-2 (KA2A5.6, Invitrogen, MA5-12748) to determine the farnesylation state of HDJ-2 after lonafarnib treatment in mice.

Overexpression and silencing of Rhes were achieved by stereotactic injections of ice-cold lactated ringer dialyzed AAVs (AAV 2/5) carrying either Rhes-IRES-GFP (Rhes), an engineered Rhes-targeted synthetic microRNA (Rhes-miR), or U6 alone to the entorhinal cortex on bregma coordinates −0.30 (anteroposterior), −2.00 (lateral), and −4.80 (dorsoventral). Stereotactic injections of $1 \times 10^9$ viral particles were performed on rTg4510 mice at 10 weeks of age. Packaged viral vectors were provided by B. Davidson (University of Pennsylvania) and kept at −80°C until dialysis.

### Sample preparation and immunocytochemistry

Animals were transcardially perfused using 4% paraformaldehyde in 0.1 M sodium cacodylate (Electron Microscopy Sciences, Hatfield, PA) for 15 min at room temperature. Brains were then dissected and immersion-fixed for 48 hours at 4°C. Immunocytochemistry was carried as described elsewhere *(55)*. Briefly, samples were rinsed 5 × 5 min in phosphate-buffered saline (PBS; pH 7.4) and then coronally sectioned at 100 μm using a vibratome (Leica, Lumberton, NJ). Sections were immersed in normal donkey serum 1:20 in PBS containing 0.5% bovine serum albumin, 0.1% Triton X-100, and 0.1% sodium azide (PBTA) at 4°C on a rotator for continuous overnight agitation followed by immersion in MC1 (provided by P. Davies, Feinstein Institute for Medical Research, Manhasset, NY; mouse monoclonal, 1:200), anti-Iba1 (Wako Laboratory Chemicals, Richmond, VA; rabbit polyclonal, 1:200), anti-GFAP (Abcam, San Francisco, CA; chicken polyclonal, 1:500), anti-RASD2 (GeneTex, Irvine, CA; GTX85428, rabbit polyclonal), anti-ubiquitin (Abcam, ab7780; rabbit polyclonal), and anti–sumo 1 (Abcam, ab11672; rabbit monoclonal) diluted in PBTA. The following day, sections were rinsed 5 × 5 min in PBTA and 1 × 1 hour in PBTA and then placed in secondary antibodies donkey anti-mouse 568, anti-rabbit 488, and anti-chicken 647 (Jackson ImmunoResearch Laboratories, West Grove, PA; 1:200). Last, secondary antibodies were rinsed and mounted using VECTASHIELD (Vector Laboratories Inc., Burlingame, CA) on a glass slide and sealed under an 18 × 18 #0 micro-coverslip (Thomas Scientific, Swedesboro, NJ) using nail polish.

### Large-scale mosaic acquisition, registration, and image analysis

Specimens were screened and imaged using an Olympus Fluoview 1000 laser scanning confocal microscope (Center Valley, PA) equipped with an argon 488-nm photodiode laser and HeNe 543/633-nm photodiode lasers as well as precision motorized stage (Applied Scientific Instrumentation Inc., Eugene, OR). Three coronal sections per mouse that spanned the hippocampal formation from anterior to posterior were selected. Mosaics were captured using an UPlanSApo 20× air lens, 0.75 numerical aperture at 1-μm intervals along the *z* axis and a pixel array of 800 × 800 in the *x-y* axes. Image stacks were collected sequentially using the Olympus Fluoview software version 4.2 with 5% overlap between individual tiles. Alignment and registration of individual tiles were performed in a semiautomated fashion by Imago 1.5 (Mayachitra Inc., Santa Barbara, CA).

Whole-brain mosaics were manually segmented into either hippocampal or cortical regions using Fiji version 2.0.0. Images were set as 8-bit, and thresholds were manually adjusted. Total number of MC1-positive neurons and Iba1-positive microglia were quantified using Fiji's Analyze Particles function *(56)*. Segmentation of anti-GFAP staining was performed using Weka *(57)*, a third-party library included in Fiji. The numbers of Rhes-positive, sumo-positive, and ubiquitin-positive cells were quantified in Fiji by discretely counting cells positively immunostained over threshold adjustments indicated above on confocal z-stacks of micrographs collected at 1024 × 1024 pixel arrays.

### Behavioral characterization

Nest shredding behavior was qualitatively measured according to published guidelines *(29)* with modifications. Briefly, unscented nestlets were provided during husbandry and kept in the cage for 24 hours. Nest shredding behavior overnight was estimated on a 0 to 5 scale, with 0 indicating unshredded bedding material and 5 denoting a completely shredded nest that displayed a rounded appearance. Twenty-five blinded independent observers reviewed images of overnight nests, and the average quality scores were calculated. After this time, a picture of the remaining nestlet or the nest was taken, and the pictures were scored on a 0 to 5 scale: 0 for an unshredded nest, 1 and 2 for nests slightly to moderately shredded, 3 and 4 for nests that were shredded but the appearance of the nest was flat, and 5 for nests that were fully shredded and the appearance of the nest was round and full. Scores of each nest were assigned blindly by 25 independent observers, and these scores were averaged to produce net-scores (Fig. 3D). Kruskal-Wallis tests followed by Wilcoxon post hoc tests were used to determine statistical significance in the difference of means.

Marble burial was evaluated as previously reported *(28)* with minor modifications as follows: 20 marbles of 15 mm in diameter were spaced by 4 cm in five rows of four marbles each on the surface of a gently packed 5-cm-deep wood chip bedding in a double-size rat cage. A mouse was left alone in the cage for 30 min and then returned to its housing cage. An observer blinded to the treatment counted the number of marbles buried. Any marble buried more than two-thirds of its size was counted. Each mouse was assessed three times on consecutive days, at the same time in the afternoon, and data were reported as average ± SEM of the percentage of buried marbles per animal. A two-way ANOVA test was used to evaluate the effect of

aging and genotype in marble burying. Kruskal-Wallis tests followed by Wilcoxon post hoc test were used to determine statistical significance of marble burying in transgenic mice treated or left untreated with lonafarnib.

rTg4510 transgenic mice displayed left-patterned accelerated gate (circling) behavior, which was often spontaneous but could also be stimulated by the presence of an observation. To quantify, mice were observed during marble burial experiments and categorically assigned to either circling or not circling categories. Circling never fully stopped during the observation period, which was longer than 5 min. The ratio of circling mice to the total number of mice was determined ($n = 6$). Statistical significance was evaluated with a two-sample test for equality of proportions without continuity correction (R, prop. test) to rTg4510 control mice.

### Evaluation of intracellular proteolysis and autophagy in lonafarnib-treated cells

Mouse fibroblasts (NIH3T3) or neuroblastoma N2a cells were obtained from the American Type Culture Collection. Cells were maintained in Dulbecco's modified Eagle's medium (DMEM) (Sigma-Aldrich, St. Louis, MO) in the presence of 10% newborn calf serum (NCS), penicillin (50 μg/ml), and streptomycin (50 μg/ml) at 37°C with 5% $CO_2$ and treated with varying concentrations of lonafarnib (0.25 to 1 μM).

Macroautophagy activity in intact cells was measured upon transduction with lentivirus carrying the mCherry-GFP-LC3 tandem construct *(32)*. Cells were plated on coverslips or glass-bottom 96-well plates, and fluorescence was read in both channels. Puncta positive for both fluorophores correspond to autophagosomes, whereas those only positive for the red fluorophore correspond to autolysosomes. Autophagic flux was determined as the conversion of autophagosomes (yellow) to autolysosomes (puncta; red). In a second set of experiments, macroautophagy activity was determined by immunoblot for LC3 (2775, Cell Signaling Technology, 1:1000) and p62 of cells exposed to inhibitors of lysosomal degradation (100 μM leupeptin/20 mM $NH_4Cl$). Autophagic flux was calculated as the increase in these two proteins in inhibitor-treated cells relative to untreated. Markers of macroautophagy were also evaluated by immunoblot for these two proteins in brain lysates from WT and rTg4510 transgenic mice treated or not with lonafarnib.

CMA activity was quantified in intact cells using the photoswitchable KFERQ-PS-Dendra2 reporter transduced into cells using lentiviral delivery *(33)*. Cells were photoswitched with a 405-nm light-emitting diode (Norlux) for 4 min with an intensity of 3.5 mA (current constant). CMA activity was quantified as the number of Dendra photoconverted positive puncta per cell. Endosomal microautophagy *(34)* activity was measured in intact cells using a recently developed N-terminal KFERQ-split-Venus and C-terminal KFERQ-split-Venus *(8)*. As the half proteins are targeted to the multivesicular bodies in late endosomes, the confined space inside these vesicles favors the interaction of the two parts, and once Venus is joined, punctate fluorescence results. The amount of reporter undergoing degradation in this compartment can be estimated by comparing the number of puncta in cells treated or not with $NH_4Cl$ and leupeptin to inhibit lumenal degradation.

To determine possible changes in proteasome-dependent degradation, cells were transduced with lentivirus carrying the degron-GFP *(35)* that will undergo rapid degradation inside cells unless lactacystin is added to inhibit proteasome activity. Rates of degradation are calculated as the increase in total cellular fluorescence upon addition of lactacystin, and discounting changes in cells transduced with lentivirus carrying a mutant-degron-GFP, unable to undergo selective proteasome degradation.

For all reporters, cells plated in glass-bottom 96-well plates were treated for the indicated times, and after fixation, images were acquired using a high-content microscope (Operetta, PerkinElmer). Images of nine different fields per well were captured, resulting in an average of 2500 to 3000 cells. Nuclei and puncta were identified using the manufacturer's software. The number of particles/puncta per cell was quantified using the "particle identifier" function in the cytosolic region after thresholding in nonsaturated images *(58)*. In all cases, focal plane thickness was set at 0.17 μm and sections with maximal nucleus diameter were selected for quantification. Values are presented as the number of puncta per cell section that, in our acquisition conditions, represents 10 to 20% of the total puncta per cell in flat cells such as NIH3T3 and 2 to 5% of the total puncta per cell in round cells such as N2a.

To measure degradation of long-lived proteins, confluent cells were labeled with [$^3$H]leucine (2 μCi/ml) for 48 hours at 37°C and then extensively washed and maintained in complete (10% NCS) or serum-deprived medium containing an excess of unlabeled leucine (2.8 mM) to prevent reutilization of radiolabeled leucine *(59)*. Aliquots of the medium taken at different times were precipitated with trichloroacetic acid, and proteolysis was measured as the percentage of the initial acid-insoluble radioactivity (protein) transformed into acid-soluble radioactivity (amino acids and small peptides) at the end of the incubation. Total radioactivity incorporated into cellular proteins was determined as the amount of acid-precipitable radioactivity in labeled cells immediately after washing.

All numerical results are reported as means ± SEM. Statistical significance of the difference between experimental groups was analyzed by two-tailed unpaired Student's *t* test. Differences were considered statistically significant for $P < 0.05$.

### Evaluation of proteolysis contribution to lonafarnib-enhanced tau degradation

Hippocampal primary mouse neuronal cocultures were prepared from E19 mouse hippocampi, dissected and dissociated with 2.5% trypsin, and plated in poly-L-lysine–coated cell culture six-well plates at a density of 250,000 neurons per well. Hippocampal neurons were matured for 3 weeks in neurobasal medium supplemented with N2, B-27, and L-glutamine with 1% penicillin and streptomycin cocktail. Neurons were fed by replacing half of the culture medium with prewarmed and freshly supplemented medium twice per week. Cells were then transduced with $1 \times 10^9$ AAV 2/5 particles per well to either overexpress or silence Rhes and simultaneously treated with lonafarnib at varying concentrations ranging from 0 to 1 μM. Cell lysates were obtained 24 hours after treatment with radioimmunoprecipitation assay buffer after adding proteasome inhibitor cocktail (cOmplete, Roche, Branford, CT) and phosphatase inhibitor cocktail (Sigma-Aldrich), as per the manufacturer's instructions. Proteins were separated with SDS-PAGE and wet-transferred to nitrocellulose. Membranes were then blotted with PHF-1 and β-actin (1:1000, each) and imaged using a LI-COR fluorescent scanner.

To dissect the contribution of diverse proteolysis pathways, hippocampal primary mouse neurons treated as described above with AAV 2/5 to overexpress Rhes in the presence of 250 nM lonafarnib were further treated in the presence of either a cocktail of 20 mM $NH_4Cl$ and 100 μM leupeptin to prevent lysosomal-mediated proteolysis or 5 μM

MG-132 to block proteasome-mediated proteolysis or were left untreated. Cell lysates were collected as described above 12 hours after treatments, or treatments were replenished at 12 hours, and lysates were collected 24 hours after treatments began. Membranes were blotted with PHF-1, p62 (ab56416, Abcam) at 1:1000, or β-tubulin III (Sigma-Aldrich) at 1:5000.

### Statistical analysis

Specific statistical analyses performed for different experimental procedures varied depending on the specific experimental technique. Therefore, the statistical methodologies are specified within the Materials and Methods subsections. In more general terms, normality assumption was tested with the Shapiro-Wilk test, where normality assumption was rejected if $P < 0.05$. When comparing averages in two groups, two-sided Student's $t$ test or Welch $t$ test was performed when normality assumption was not rejected, and Mann-Whitney $U$ test was performed otherwise. For comparing averages on multiple groups, one-way ANOVA followed by Tukey's HSD post hoc tests were evaluated if the normality assumption was not rejected, and Kruskal-Wallis tests followed by Wilcoxon tests were used otherwise. To assess the effect on a dependent variable when two independent variables such as age and phenotype were measured, two-way ANOVA tests were performed. Differences in the mean were considered to be significant when $P < 0.05$, and degree of significance was reported with $^{*}P < 0.05$, $^{**}P < 0.01$, $^{***}P < 0.001$, and $^{****}P < 1 \times 10^{-4}$, respectively.

For experiments involving mice, sample size ($n$) and female:male ratios used at each experiment are indicated in the figure legends. Power analysis was performed to verify that a power greater than 0.80 was obtained while minimizing unnecessary animal usage in replication. For experiments using cell lines or hiPSC-derived neuron cultures, the number of independent biological replicates is reported ($N$).

## SUPPLEMENTARY MATERIALS

www.sciencetranslationalmedicine.org/cgi/content/full/11/485/eaat3005/DC1
Materials and Methods
Fig. S1. Tau pathology progression in rTg4510 transgenic mice.
Fig. S2. PHF-1 immunoreactivity is reduced by lonafarnib treatment.
Fig. S3. Acute treatment of lonafarnib does not alter tau pathology in aged rTg4510 transgenic mice.
Fig. S4. Effect of lonafarnib in macroautophagy and CMA.
Fig. S5. Farnesyltransferase activity inhibition activates autophagy.
Fig. S6. Sumo and ubiquitin are reduced by lonafarnib and Rhes-miR treatments.
Fig. S7. Lonafarnib's effect on Rhes localization.
Fig. S8. Degradation of Rhes is insensitive to lysosomal proteolysis blocking.
Fig. S9. Lonafarnib treatment is effective in reducing phospho-tau in iPSC-derived neurons.
Fig. S10. Transcriptomic analysis of hiPSC-derived neurons harboring tau mutations.
Fig. S11. Ubiquitinated and sumoylated tau are not altered by lonafarnib treatment.
Fig. S12. Model for a Rhes pathway mechanism.
Movie S1. Lonafarnib attenuates behavioral circling in rTg4510 (mp4).
Data file S1: Differentially expressed genes in hiPSC-derived neurons with MAPT variants (Excel file).
Data file S2. Quantification data for rTg4510-treated mice (excel file).
References (*61*–*65*)

## REFERENCES AND NOTES


1. C. U. Onyike, J. Diehl-Schmid, The epidemiology of frontotemporal dementia. *Int. Rev. Psychiatry* **25**, 130–137 (2013).
2. J. Götz, A. Ittner, L. M. Ittner, Tau-targeted treatment strategies in Alzheimer's disease. *Br. J. Pharmacol.* **165**, 1246–1259 (2012).
3. S. L. DeVos, R. L. Miller, K. M. Schoch, B. B. Holmes, C. S. Kebodeaux, A. J. Wegener, G. Chen, T. Shen, H. Tran, B. Nichols, T. A. Zanardi, H. B. Kordasiewicz, E. E. Swayze, C. F. Bennett, M. I. Diamond, T. M. Miller, Tau reduction prevents neuronal loss and reverses pathological tau deposition and seeding in mice with tauopathy. *Sci. Transl. Med.* **9**, eaag0481 (2017).
4. E. Mead, D. Kestoras, Y. Gibson, L. Hamilton, R. Goodson, S. Jones, S. Eversden, P. Davies, M. O'Neill, M. Hutton, P. Szekeres, J. Wolak, Halting of Caspase activity protects tau from MC1-conformational change and aggregation. *J. Alzheimers Dis.* **54**, 1521–1538 (2016).
5. K. Hochgräfe, A. Sydow, D. Matenia, D. Cadinu, S. Könen, O. Petrova, M. Pickhardt, P. Goll, F. Morellini, E. Mandelkow, E.-M. Mandelkow, Preventive methylene blue treatment preserves cognition in mice expressing full-length pro-aggregant human tau. *Acta Neuropathol. Commun.* **3**, 25 (2015).
6. X. Zhang, I. Hernandez, D. Rei, W. Mair, J. K. Laha, M. E. Cornwell, G. D. Cuny, L.-H. Tsai, J. A. J. Steen, K. S. Kosik, Diaminothiazoles modify tau phosphorylation and improve the tauopathy in mouse models. *J. Biol. Chem.* **288**, 22042–22056 (2013).
7. S.-W. Min, X. Chen, T. E. Tracy, Y. Li, Y. Zhou, C. Wang, K. Shirakawa, S. S. Minami, E. Defensor, S. A. Mok, P. D. Sohn, B. Schilling, X. Cong, L. Ellerby, B. W. Gibson, J. Johnson, N. Krogan, M. Shamloo, J. Gestwicki, E. Masliah, E. Verdin, L. Gan, Critical role of acetylation in tau-mediated neurodegeneration and cognitive deficits. *Nat. Med.* **21**, 1154–1162 (2015).
8. B. Caballero, Y. Wang, A. Diaz, I. Tasset, Y. R. Juste, B. Stiller, E.-M. Mandelkow, E. Mandelkow, A. M. Cuervo, Interplay of pathogenic forms of human tau with different autophagic pathways. *Aging Cell* **17**, e12692 (2018).
9. J. L. Guo, A. Buist, A. Soares, K. Callaerts, S. Calafate, F. Stevenaert, J. P. Daniels, B. E. Zoll, A. Crowe, K. R. Brunden, D. Moechars, V. M. Y. Lee, The dynamics and turnover of tau aggregates in cultured cells: Insights into therapies for tauopathies. *J. Biol. Chem.* **291**, 13175–13193 (2016).
10. A. Lopez, S. E. Lee, K. Wojta, E. M. Ramos, E. Klein, J. Chen, A. L. Boxer, M. L. Gorno-Tempini, D. H. Geschwind, L. Schlotawa, N. V. Ogryzko, E. H. Bigio, E. Rogalski, S. Weintraub, M. M. Mesulam, Tauopathy Genetics Consortium, A. Fleming, G. Coppola, B. L. Miller, D. C. Rubinsztein, A152T tau allele causes neurodegeneration that can be ameliorated in a zebrafish model by autophagy induction. *Brain* **140**, 1128–1146 (2017).
11. R. A. Nixon, The role of autophagy in neurodegenerative disease. *Nat. Med.* **19**, 983–997 (2013).
12. M. C. Chang, K. Srinivasan, B. A. Friedman, E. Suto, Z. Modrusan, W. P. Lee, J. S. Kaminker, D. V. Hansen, M. Sheng, Progranulin deficiency causes impairment of autophagy and TDP-43 accumulation. *J. Exp. Med.* **214**, 2611–2628 (2017).
13. M. P. Nelson, M. Boutin, T. E. Tse, H. Lu, E. D. Haley, X. Ouyang, J. Zhang, C. Auray-Blais, J. J. Shacka, The lysosomal enzyme alpha-galactosidase A is deficient in Parkinson's disease brain in association with the pathologic accumulation of alpha-synuclein. *Neurobiol. Dis.* **110**, 68–81 (2018).
14. J. Colicelli, Human RAS superfamily proteins and related GTPases. *Sci. STKE* **2004**, RE13 (2004).
15. D. Spano, I. Branchi, A. Rosica, M. T. Pirro, A. Riccio, P. Mithbaokar, A. Affuso, C. Arra, P. Campolongo, D. Terracciano, V. Macchia, J. Bernal, E. Alleva, R. Di Lauro, Rhes is involved in striatal function. *Mol. Cell. Biol.* **24**, 5788–5796 (2004).
16. D. Vitucci, A. Di Giorgio, F. Napolitano, B. Pelosi, G. Blasi, F. Errico, M. T. Attrotto, B. Gelao, L. Fazio, P. Taurisano, A. Di Maio, V. Marsili, M. Pasqualetti, A. Bertolino, A. Usiello, Rasd2 modulates prefronto-striatal phenotypes in humans and "schizophrenia-like behaviors" in mice. *Neuropsychopharmacology* **41**, 916–927 (2016).
17. R. G. Mealer, A. J. Murray, N. Shahani, S. Subramaniam, S. H. Snyder, Rhes, a striatal-selective protein implicated in Huntington disease, binds beclin-1 and activates autophagy. *J. Biol. Chem.* **289**, 3547–3554 (2014).
18. S. Subramaniam, K. M. Sixt, R. Barrow, S. H. Snyder, Rhes, a striatal specific protein, mediates mutant-huntingtin cytotoxicity. *Science* **324**, 1327–1330 (2009).
19. J. Pan, E. Song, C. Cheng, M.-H. Lee, S.-C. J. Yeung, Farnesyltransferase inhibitors-induced autophagy: Alternative mechanisms? *Autophagy* **5**, 129–131 (2009).
20. L. B. Gordon, J. Massaro, R. B. D'Agostino Sr., S. E. Campbell, J. Brazier, W. T. Brown, M. E. Kleinman, M. W. Kieran, Progeria Clinical Trials Collaborative, Impact of farnesylation inhibitors on survival in Hutchinson-Gilford progeria syndrome. *Circulation* **130**, 27–34 (2014).
21. M. W. Kieran, R. J. Packer, A. Onar, S. M. Blaney, P. Phillips, I. F. Pollack, J. R. Geyer, S. Gururangan, A. Banerjee, S. Goldman, C. D. Turner, J. B. Belasco, A. Broniscer, Y. Zhu, E. Frank, P. Kirschmeier, P. Statkevich, A. Yver, J. M. Boyett, L. E. Kun, Phase I and pharmacokinetic study of the oral farnesyltransferase inhibitor lonafarnib administered twice daily to pediatric patients with advanced central nervous system tumors using a modified continuous reassessment method: A Pediatric Brain Tumor Consortium study. *J. Clin. Oncol.* **25**, 3137–3143 (2007).
22. S. Yust-Katz, D. Liu, Y. Yuan, V. Liu, S. Kang, M. Groves, V. Puduvalli, V. Levin, C. Conrad, H. Colman, S. Hsu, W. K. A. Yung, M. R. Gilbert, Phase 1/1b study of lonafarnib and temozolomide in patients with recurrent or temozolomide refractory glioblastoma. *Cancer* **119**, 2747–2753 (2013).
23. A. Desjardins, D. A. Reardon, K. B. Peters, S. Threatt, A. D. Coan, J. E. Herndon II, A. H. Friedman, H. S. Friedman, J. J. Vredenburgh, A phase I trial of the farnesyl transferase

inhibitor, SCH 66336, with temozolomide for patients with malignant glioma. *J. Neurooncol.* **105**, 601–606 (2011).
24. K. Santacruz, J. Lewis, T. Spires, J. Paulson, L. Kotilinek, M. Ingelsson, A. Guimaraes, M. DeTure, M. Ramsden, E. McGowan, C. Forster, M. Yue, J. Orne, C. Janus, A. Mariash, M. Kuskowski, B. Hyman, M. Hutton, K. H. Ashe, Tau suppression in a neurodegenerative mouse model improves memory function. *Science* **309**, 476–481 (2005).
25. N. Menkes-Caspi, H. G. Yamin, V. Kellner, T. L. Spires-Jones, D. Cohen, E. A. Stern, Pathological tau disrupts ongoing network activity. *Neuron* **85**, 959–966 (2015).
26. J. L. Crimins, A. B. Rocher, J. I. Luebke, Electrophysiological changes precede morphological changes to frontal cortical pyramidal neurons in the rTg4510 mouse model of progressive tauopathy. *Acta Neuropathol.* **124**, 777–795 (2012).
27. G. Liu, S. A. Taylor, C. H. Marrinan, Y. Hsieh, W. R. Bishop, P. Kirschmeier, B. J. Long, Continuous and intermittent dosing of lonafarnib potentiates the therapeutic efficacy of docetaxel on preclinical human prostate cancer models. *Int. J. Cancer* **125**, 2711–2720 (2009).
28. R. M. J. Deacon, Digging and marble burying in mice: Simple methods for in vivo identification of biological impacts. *Nat. Protoc.* **1**, 122–124 (2006).
29. R. M. J. Deacon, Assessing nest building in mice. *Nat. Protoc.* **1**, 1117–1119 (2006).
30. D. Gabriel, D. D. Shafry, L. B. Gordon, K. Djabali, Intermittent treatment with farnesyltransferase inhibitor and sulforaphane improves cellular homeostasis in Hutchinson-Gilford progeria fibroblasts. *Oncotarget* **8**, 64809–64826 (2017).
31. J. W. Wojtkowiak, K. M. Sane, M. Kleinman, B. F. Sloane, J. J. Reiners Jr., R. R. Mattingly, Aborted autophagy and nonapoptotic death induced by farnesyl transferase inhibitor and lovastatin. *J. Pharmacol. Exp. Ther.* **337**, 65–74 (2011).
32. S. Kimura, T. Noda, T. Yoshimori, Dissection of the autophagosome maturation process by a novel reporter protein, tandem fluorescent-tagged LC3. *Autophagy* **3**, 452–460 (2007).
33. H. Koga, M. Martinez-Vicente, F. Macian, V. V. Verkhusha, A. M. Cuervo, A photoconvertible fluorescent reporter to track chaperone-mediated autophagy. *Nat. Commun.* **2**, 386 (2011).
34. R. Sahu, S. Kaushik, C. C. Clement, E. S. Cannizzo, B. Scharf, A. Follenzi, I. Potolicchio, E. Nieves, A. M. Cuervo, L. Santambrogio, Microautophagy of cytosolic proteins by late endosomes. *Dev. Cell* **20**, 131–139 (2011).
35. R. Greussing, H. Unterluggauer, R. Koziel, A. B. Maier, P. Jansen-Dürr, Monitoring of ubiquitin-proteasome activity in living cells using a Degron (dgn)-destabilized green fluorescent protein (GFP)-based reporter protein. *J. Vis. Exp.* e3327 (2012).
36. H.-B. Luo, Y.-Y. Xia, X.-J. Shu, Z.-C. Liu, Y. Feng, X.-H. Liu, G. Yu, G. Yin, Y.-S. Xiong, K. Zeng, J. Jiang, K. Ye, X.-C. Wang, J.-Z. Wang, SUMOylation at K340 inhibits tau degradation through deregulating its phosphorylation and ubiquitination. *Proc. Natl. Acad. Sci. U.S.A.* **111**, 16586–16591 (2014).
37. L. Petrucelli, D. Dickson, K. Kehoe, J. Taylor, H. Snyder, A. Grover, M. De Lucia, E. McGowan, J. Lewis, G. Prihar, J. Kim, W. H. Dillmann, S. E. Browne, A. Hall, R. Voellmy, Y. Tsuboi, T. M. Dawson, B. Wolozin, J. Hardy, M. Hutton, CHIP and Hsp70 regulate tau ubiquitination, degradation and aggregation. *Hum. Mol. Genet.* **13**, 703–714 (2004).
38. P. Vargiu, R. D. Abajo, J. A. Garcia-Ranea, A. Valencia, P. Santisteban, P. Crespo, J. Bernal, The small GTP-binding protein, Rhes, regulates signal transduction from G protein-coupled receptors. *Oncogene* **23**, 559–568 (2004).
39. M. G. Spillantini, M. Goedert, Tau pathology and neurodegeneration. *Lancet Neurol.* **12**, 609–622 (2013).
40. A. Iyer, N. E. Lapointe, K. Zielke, M. Berdynski, E. Guzman, A. Barczak, M. Chodakowska-Zebrowska, M. Barcikowska, S. Feinstein, C. Zekanowski, A novel MAPT mutation, G55R, in a frontotemporal dementia patient leads to altered tau function. *PLOS ONE* **8**, e76409 (2013).
41. M. Hutton, C. L. Lendon, P. Rizzu, M. Baker, S. Froelich, H. Houlden, S. Pickering-Brown, S. Chakraverty, A. Isaacs, A. Grover, J. Hackett, J. Adamson, S. Lincoln, D. Dickson, P. Davies, R. C. Petersen, M. Stevens, E. de Graaff, E. Wauters, J. van Baren, M. Hillebrand, M. Joosse, J. M. Kwon, P. Nowotny, L. K. Che, J. Norton, J. C. Morris, L. A. Reed, J. Trojanowski, H. Basun, L. Lannfelt, M. Neystat, S. Fahn, F. Dark, T. Tannenberg, P. R. Dodd, N. Hayward, J. B. J. Kwok, P. R. Schofield, A. Andreadis, J. Snowden, D. Craufurd, D. Neary, F. Owen, B. A. Oostra, J. Hardy, A. Goate, J. van Swieten, D. Mann, T. Lynch, P. Heutink, Association of missense and 5′-splice-site mutations in tau with the inherited dementia FTDP-17. *Nature* **393**, 702–705 (1998).
42. M. Hasegawa, M. J. Smith, M. Goedert, Tau proteins with FTDP-17 mutations have a reduced ability to promote microtubule assembly. *FEBS Lett.* **437**, 207–210 (1998).
43. M. DeJesus-Hernandez, I. R. Mackenzie, B. F. Boeve, A. L. Boxer, M. Baker, N. J. Rutherford, A. M. Nicholson, N. A. Finch, H. Flynn, J. Adamson, N. Kouri, A. Wojtas, P. Sengdy, G.-Y. R. Hsiung, A. Karydas, W. W. Seeley, K. A. Josephs, G. Coppola, D. H. Geschwind, Z. K. Wszolek, H. Feldman, D. S. Knopman, R. C. Petersen, B. L. Miller, D. W. Dickson, K. B. Boylan, N. R. Graff-Radford, R. Rademakers, Expanded GGGGCC hexanucleotide repeat in noncoding region of *C9ORF72* causes chromosome 9p-linked FTD and ALS. *Neuron* **72**, 245–256 (2011).
44. B. Zhou, W. H. Wong, A bootstrap-based non-parametric ANOVA method with applications to factorial microarray data. *Stat. Sin.* **21**, 495 (2011).
45. D. C. Carrettiero, I. Hernandez, P. Neveu, T. Papagiannakopoulos, K. S. Kosik, The cochaperone BAG2 sweeps paired helical filament- insoluble tau from the microtubule. *J. Neurosci.* **29**, 2151–2161 (2009).
46. V. Schaeffer, I. Lavenir, S. Ozcelik, M. Tolnay, D. T. Winkler, M. Goedert, Stimulation of autophagy reduces neurodegeneration in a mouse model of human tauopathy. *Brain* **135**, 2169–2177 (2012).
47. J. Jang, Y. Wang, H.-S. Kim, M. A. Lalli, K. S. Kosik, Nrf2, a regulator of the proteasome, controls self-renewal and pluripotency in human embryonic stem cells. *Stem Cells* **32**, 2616–2625 (2014).
48. R. I. Morimoto, A. M. Cuervo, Proteostasis and the aging proteome in health and disease. *J. Gerontol. A Biol. Sci. Med. Sci.* **69** (suppl. 1), S33–S38 (2014).
49. J. H. Lee, L. Tecedor, Y. H. Chen, A. M. Monteys, M. J. Sowada, L. M. Thompson, B. L. Davidson, Reinstating aberrant mTORC1 activity in Huntington's disease mice improves disease phenotypes. *Neuron* **85**, 303–315 (2015).
50. F. Napolitano, E. Booth Warren, S. Migliarini, D. Punzo, F. Errico, Q. Li, M.-L. Thiolat, A. L. Vescovi, P. Calabresi, E. Bezard, M. Morelli, C. Konradi, M. Pasqualetti, A. Usiello, Decreased Rhes mRNA levels in the brain of patients with Parkinson's disease and MPTP-treated macaques. *PLOS ONE* **12**, e0181677 (2017).
51. P. A. Desplats, K. E. Kass, T. Gilmartin, G. D. Stanwood, E. L. Woodward, S. R. Head, J. G. Sutcliffe, E. A. Thomas, Selective deficits in the expression of striatal-enriched mRNAs in Huntington's disease. *J. Neurochem.* **96**, 743–757 (2006).
52. T. Seredenina, O. Gokce, R. Luthi-Carter, Decreased striatal RGS2 expression is neuroprotective in Huntington's disease (HD) and exemplifies a compensatory aspect of HD-induced gene regulation. *PLOS ONE* **6**, e22231 (2011).
53. V. Prahlad, R. I. Morimoto, Integrating the stress response: Lessons for neurodegenerative diseases from *C. elegans*. *Trends Cell Biol.* **19**, 52–61 (2009).
54. C. Voisine, J. S. Pedersen, R. I. Morimoto, Chaperone networks: Tipping the balance in protein folding diseases. *Neurobiol. Dis.* **40**, 12–20 (2010).
55. G. Luna, S. Kjellstrom, M. R. Verardo, G. P. Lewis, J. Byun, P. A. Sieving, S. K. Fisher, The effects of transient retinal detachment on cavity size and glial and neural remodeling in a mouse model of X-linked retinoschisis. *Invest. Ophthalmol. Vis. Sci.* **50**, 3977–3984 (2009).
56. J. Schindelin, I. Arganda-Carreras, E. Frise, V. Kaynig, M. Longair, T. Pietzsch, S. Preibisch, C. Rueden, S. Saalfeld, B. Schmid, J.-Y. Tinevez, D. J. White, V. Hartenstein, K. Eliceiri, P. Tomancak, A. Cardona, Fiji: An open-source platform for biological-image analysis. *Nat. Methods* **9**, 676–682 (2012).
57. I. Arganda-Carreras, V. Kaynig, C. Rueden, K. W. Eliceiri, J. Schindelin, A. Cardona, H. S. Seung, Trainable Weka segmentation: A machine learning tool for microscopy pixel classification. *Bioinformatics* **33**, 2424–2426 (2017).
58. S. Kaushik, A. M. Cuervo, Chapter 19 methods to monitor chaperone-mediated autophagy. *Methods Enzymol.* **452**, 297–324 (2009).
59. J. S. Auteri, A. Okada, V. Bochaki, J. F. Dice, Regulation of intracellular protein degradation in IMR-90 human diploid fibroblasts. *J. Cell. Physiol.* **115**, 167–174 (1983).
60. D. Kim, G. Pertea, C. Trapnell, H. Pimentel, R. Kelley, S. L. Salzberg, TopHat2: Accurate alignment of transcriptomes in the presence of insertions, deletions and gene fusions. *Genome Biol.* **14**, R36 (2013).
61. H. Li, B. Handsaker, A. Wysoker, T. Fennell, J. Ruan, N. Homer, G. Marth, G. Abecasis, R. Durbin, 1000 Genome Project Data Processing Subgroup, The Sequence Alignment/Map format and SAMtools. *Bioinformatics* **25**, 2078–2079 (2009).
62. K. D. Pruitt, J. Harrow, R. A. Harte, C. Wallin, M. Diekhans, D. R. Maglott, S. Searle, C. M. Farrell, J. E. Loveland, B. J. Ruef, E. Hart, M.-M. Suner, M. J. Landrum, B. Aken, S. Ayling, R. Baertsch, J. Fernandez-Banet, J. L. Cherry, V. Curwen, M. DiCuccio, M. Kellis, J. Lee, M. F. Lin, M. Schuster, A. Shkeda, C. Amid, G. Brown, O. Dukhanina, A. Frankish, J. Hart, B. L. Maidak, J. Mudge, M. R. Murphy, T. Murphy, J. Rajan, B. Rajput, L. D. Riddick, C. Snow, C. Steward, D. Webb, J. A. Weber, L. Wilming, W. Wu, E. Birney, D. Haussler, T. Hubbard, J. Ostell, R. Durbin, D. Lipman, The consensus coding sequence (CCDS) project: Identifying a common protein-coding gene set for the human and mouse genomes. *Genome Res.* **19**, 1316–1323 (2009).
63. M. D. Robinson, D. J. McCarthy, G. K. Smyth, edgeR: A Bioconductor package for differential expression analysis of digital gene expression data. *Bioinformatics* **26**, 139–140 (2009).
64. D. J. McCarthy, Y. Chen, G. K. Smyth, Differential expression analysis of multifactor RNA-Seq experiments with respect to biological variation. *Nucleic Acids Res.* **40**, 4288–4297 (2012).
65. M. E. Ritchie, B. Phipson, D. Wu, Y. Hu, C. W. Law, W. Shi, G. K. Smyth, *limma* powers differential expression analyses for RNA-sequencing and microarray studies. *Nucleic Acids Res.* **43**, e47 (2015).

**Acknowledgments:** We thank B. Davidson for designing and packaging AAVs used in this study; P. Davies for providing MC1, PHF-1, and ET3 antibodies; and Y. Huang for reprogramming CTR2 and CTR3 iPSC lines. We thank the NINDS Cell Repository for the fibroblast lines from the *MAPT* P301L and V337M mutation carriers, as well as H.-S. Kim and C. Park for reprogramming the *MAPT*-G55R iPSC line. We also thank P. Lansbury and M. Duggan for providing lonafarnib plasma and brain concentrations after oral administration to mice. **Funding:** This work was

funded by the Tau Consortium (K.S.K., A.M.C., A.M.G., and C.M.K.); NIH grants 1U54NS100717 (K.S.K. and A.M.C.), R01AG056058 (K.S.K.), R01AG054008 (A.M.G.), and AG046374 (C.M.K.); NSF grant ISS-0808772 and Information Technology Research (ITR) grant 0331697 (S.K.F.); Cohen Veterans Bioscience (K.S.K.); and the Leo and Ann Albert Charitable Trust (K.S.K.). N.J.S. was supported by a postdoctoral EMBO fellowship. **Author contributions:** I.H. and G.L. designed and performed experiments and wrote the manuscript. I.H. performed the statistical analyses. J.N.R., S.A.R., and S.J.H. performed experiments on Rhes biochemistry. M.G. performed mouse experiments and maintained colonies. D.B. and Y.E.S. performed immunohistochemistry and microscopy experiments. A.A.K. performed computational quantifications of brain micrographs and mosaics. C.R.H. and V.C. performed neuronal differentiation from hiPSCs. E.G. performed IonTorrent sequencing for RNAseq experiments. H.Z. performed RNA sequence mapping and quality control. C.M.K. and A.M.G. contributed isogenic neuron complementary DNA for Rhes quantitation and iPSC line generation. C.Z. identified patients with frontotemporal dementia carrying the MAPT-G55R mutation, collected skin fibroblasts, and prepared primary fibroblast cultures. N.J.S., A.D., S.K., and A.M.C. designed and performed experiments of lonafarnib's effects in proteolysis and lysosomes. S.K.F. performed image analysis and critiqued the manuscript. K.S.K. conceived the experiments and wrote the manuscript. **Competing interests:** K.S.K. consults for ADRx. A.M.C. is cofounder of Selphagy. A.M.G. has served on the scientific advisory board of Denali Therapeutics (2015–2018) and has consulted for Cognition Therapeutics, AbbVie, Eisai, Biogen, GSK, and Pfizer. S.J.H. has consulted for Rodin Therapeutics, Frequency Therapeutics, Psy Therapeutics, and AstraZeneca and has received speaker fees from Amgen and Merck. K.S.K. and I.H. are coinventors on patent no. US2018/013712 entitled "Treatment of neurodegenerative conditions by disruption of Rhes." **Data and materials availability:** All data associated with this paper are in the main text or Supplementary Materials. hiPSCs used in this study were obtained under material transfer agreements executed at UCSB (Kosik-Huang, 014344-0002, and 014344-0003). All digital image datasets used for spatial analyses have been deposited to BisQue (Bio-Image Semantic Query User Environment) *(60)* and are publically available for further use with permission: https://bisque.ece.ucsb.edu/client_service/view?resource=https://bisque.ece.ucsb.edu/data_service/00-iZXFv5ELXaikLmi2viaSRJ.

Submitted 14 February 2018
Resubmitted 15 August 2018
Accepted 30 November 2018
Published 27 March 2019
10.1126/scitranslmed.aat3005

**Citation:** I. Hernandez, G. Luna, J. N. Rauch, S. A. Reis, M. Giroux, C. M. Karch, D. Boctor, Y. E. Sibih, N. J. Storm, A. Diaz, S. Kaushik, C. Zekanowski, A. A. Kang, C. R. Hinman, V. Cerovac, E. Guzman, H. Zhou, S. J. Haggarty, A. M. Goate, S. K. Fisher, A. M. Cuervo, K. S. Kosik, A farnesyltransferase inhibitor activates lysosomes and reduces tau pathology in mice with tauopathy. *Sci. Transl. Med.* **11**, eaat3005 (2019).

# Abstract

**One-sentence summary:** Targeting farnesylation of Rhes induces lysosomal-mediated tau degradation and reduces tau pathology in mice with tauopathy.

**Editor's Summary:**
**A rheostat for tau pathology**

Tau inclusions are a prominent feature of many neurodegenerative diseases and are considered to be a potential therapeutic target. Hernandez *et al.* now report a previously unrecognized pathway leading to tau clearance via the lysosome. Activation of this pathway by inhibiting the enzyme farnesyltransferase blocks the attachment of a neuronal protein, Rhes, to the cell membrane. Farnesyltransferase inhibitors are already in use in human patients for treating cancer. The authors treated a mouse model of tauopathy with one such drug, lonafarnib, and were able to prevent the formation of tau inclusions, decrease microgliosis and brain atrophy, and attenuate behavioral abnormalities.